0 4 APR 2000

AFRL-ML-WP-TR-1999-4140

HIGH PERFORMANCE FLAT COATINGS THROUGH COMPATIBILIZED IMMISCIBLE POLYMER BLENDS

T.J. FABISH
W.F. LYNN
R.J. PASSINAULT
A. VREUGDENHIL
B. METZ
V. McGINNISS

SYSTRAN FEDERAL CORPORATION
4126 LINDEN AVENUE
DAYTON, OH 45432

JULY 1999

FINAL REPORT FOR NOV 1998 – JUL 1999

20000410 187

MATERIALS AND MANUFACTURING DIRECTORATE
AIR FORCE RESEARCH LABORATORY
AIR FORCE MATERIEL COMMAND
WRIGHT-PATTERSON AIR FORCE BASE OH 45433-7750

DTIC QUALITY INSPECTED 1

NOTICE

USING GOVERNMENT DRAWINGS, SPECIFICATIONS, OR OTHER DATA INCLUDED IN THIS DOCUMENT FOR ANY PURPOSE OTHER THAN GOVERNMENT PROCUREMENT DOES NOT IN ANY WAY OBLIGATE THE US GOVERNMENT. THE FACT THAT THE GOVERNMENT FORMULATED OR SUPPLIED THE DRAWINGS, SPECIFICATIONS, OR OTHER DATA DOES NOT LICENSE THE HOLDER OR ANY OTHER PERSON OR CORPORATION; OR CONVEY ANY RIGHTS OR PERMISSION TO MANUFACTURE, USE, OR SELL ANY PATENTED INVENTION THAT MAY RELATE TO THEM.

THIS REPORT IS RELEASABLE TO THE NATIONAL TECHNICAL INFORMATION SERVICE (NTIS). AT NTIS, IT WILL BE AVAILABLE TO THE GENERAL PUBLIC, INCLUDING FOREIGN NATIONS.

THIS TECHNICAL REPORT HAS BEEN REVIEWED AND IS APPROVED FOR PUBLICATION.

STEPHEN L. SZARUGA, Act Chief
Nonstructural Materials Branch
Nonmetallic Materials Division

ROGER D. GRISWOLD, Asst Chief
Nonmetallic Materials Division
Materials & Manufacturing Directorate

Do not return copies of this report unless contractual obligations or notice on a specific document requires its return.

REPORT DOCUMENTATION PAGE

1. AGENCY USE ONLY (Leave blank)	2. REPORT DATE	3. REPORT TYPE AND DATES COVERED
	JULY 1999	FINAL REPORT FOR NOV 1998 - JUL 1999

4. TITLE AND SUBTITLE
HIGH PERFORMANCE FLAT COATINGS THROUGH COMPATIBILIZED IMMISCIBLE POLYMER BLENDS

5. FUNDING NUMBERS
C   F33615-94-C-5804
PE   62102
PR   4347
TA   60
WU   FJ

6. AUTHOR(S)
T.J. FABISH, W.F. LYNN, R.J. PASSINAULT
A. VREUGDENHIL, B. METZ , V. McGINNISS

7. PERFORMING ORGANIZATION NAME(S) AND ADDRESS(ES)
SYSTRAN FEDERAL CORPORATION
4126 LINDEN AVENUE
DAYTON, OHIO 45432

8. PERFORMING ORGANIZATION REPORT NUMBER

9. SPONSORING/MONITORING AGENCY NAME(S) AND ADDRESS(ES)
MATERIALS AND MANUFACTURING DIRECTORATE
AIR FORCE RESEARCH LABORATORY
AIR FORCE MATERIEL COMMAND
WRIGHT-PATTERSON AFB, OH 45433-7750
POC: STEPHEN L. SZARUGA, AFRL/MLBT, 937-255-4860

10. SPONSORING/MONITORING AGENCY REPORT NUMBER
AFRL-ML-WP-TR-1999-4140

11. SUPPLEMENTARY NOTES

12a. DISTRIBUTION AVAILABILITY STATEMENT

APPROVED FOR PUBLIC RELEASE, DISTRIBUTION UNLIMITED.

12b. DISTRIBUTION CODE

13. ABSTRACT (Maximum 200 words)

A new approach to high performance ultra low gloss aircraft coating systems is described based on compatibilized immiscible blends of two polyols that differ significantly in surface energy. Extensive characterization measurements show the performance of the polymer alloy systems surpasses existing benchmark polyurethane and fluoropolymer topcoat systems in hardness, chemical resistance, fluid resistance, abrasion resistance, and cleanability. The superior performance in screening tests is attributed to a favorable synergism between the parent homopolymers that is enabled by the stress bearing interface and morphology peculiar to an alloy. A method is explored for connecting a standard coating screening test to the more fundamental linear response coefficients measured in thin film dynamic mechanical analysis (DMA). An extension is proposed aimed at utilizing the thermodynamic drive arising from the difference in component surface energies to assemble pigments in threadlike fashion through one polymer phase to prescribe effective medium optical properties at minimal pigment loading.

14. SUBJECT TERMS

15. NUMBER OF PAGES
66

16. PRICE CODE

17. SECURITY CLASSIFICATION OF REPORT	18. SECURITY CLASSIFICATION OF THIS PAGE	19. SECURITY CLASSIFICATION OF ABSTRACT	20. LIMITATION OF ABSTRACT
UNCLASSIFIED	UNCLASSIFIED	UNCLASSIFIED	SAR

Table of Contents

List of Figures

List of Figures-continued

List of Figures-continued

List of Tables

1. Introduction

a. The Coating Challenge

Air Force aircraft operate in climates ranging from arctic to tropical. A single flight may present extremes in temperature and pressure excursions and in erosive water, particulate, and solar radiation exposures far beyond any originating with climate. Aircraft coatings are expected to protect the structure against the environment while maintaining aesthetic appearance. A pressing challenge to coating formulation is achieving Air Force ultra-low matte finish requirements *and* corrosion resistance, toughness, and durability. For example, certain Air Force applications require 60° and 85° gloss less than 5 and a film durability of 5 to 12 years before recoat. Movement to the higher performance level may require innovation well beyond current paint technology. A promising materials strategy for high performance, ultra low gloss topcoat systems is described in this report.

b. Role of Extender Pigment in Optical Properties in the Visible and IR

Low gloss Air Force coatings have traditionally been formulated using high volume concentrations of extender pigments. Extender pigments can act as surface roughening agents and light scattering sites. Also, high energy absorption at visible and IR energies is desired for a low gloss protective coating. A brief consideration of the steady state of a beam of visible/IR radiant energy incident on a coating can provide useful insight into roles played by pigment structure and size in energy absorption.

A fraction of an electromagnetic wave incident on a surface will be reflected and the remaining wave intensity will propagate through the surface and into the bulk of the film. A fraction of the propagating energy is absorbed through the action of microscopic processes that convert electromagnetic energy into thermal energy. A fraction of the wave intensity arriving at the substrate may transit the substrate and leave the coating system while the remainder is reflected back into the bulk of the film to propagate towards the front surface. A fraction of this propagating energy exits the system at the front surface to comprise a component of the net reflected wave while the remainder is reflected back into the bulk to undergo absorption in transit and another transmission/reflection division at the substrate. Summing over the multiple reflections at all surfaces according to the local amplitude reflection coefficient and including energy absorption between reflections results in the familiar relationships that resolve the radiant power incident on a structure into reflected, absorbed, and transmitted components. A surface that is rough on the scale of the radiation wavelength will diffuse the reflected power. Specular components will introduce a pronounced dependence of reflected power on the angle between the incident and reflected wave.

The radiant energy absorption process may be described classically through an effective Beer's law, $A = \log(E\ p\ c)$, where E is the effective medium extinction coefficient of the material, p is the path length, and c is the concentration of all absorbing species. E in the Beer's law relation is directly related to the effective medium absorption coefficient, or equivalently, to the imaginary term in the particular optical response function that is

invoked in the continuum model description. It is evident that an extender pigment can directly contribute to energy absorption through its structure providing strong coupling to the electromagnetic radiation field via, for example, a large permanent or dynamic electric dipole moment. The extender pigment can also affect energy absorption through its size. Particle size may be selected with guidance from Mie theory to maximally scatter incident radiant energy within a selected wavelength region thereby increasing path length. Prime pigments can scatter efficiently through the visible, while larger extender pigments can scatter into the IR region. Traditional coating strategy relies on scattering and absorption by extender pigments to achieve low gloss. Extender pigments are low cost, particulate, filler materials that can impart other advantageous properties like hardness and scrub and mar resistance to a coating in addition to aiding control of optical properties. Experience teaches, however, that a number of physical properties of the film become compromised when the coating is formulated with a PVC (the ratio of pigment volume to total solids volume) too near CPVC (the 'Critical' PVC where pigment particles first touch to form a continuous network). For example, too large an extender size compromises surface finish and too high loading compromises film integrity. Extreme flattening through pigmentation usually necessitates PVC very near CPVC.

c. Role of Extender Pigment in Aging and Weathering

High levels of extender pigment can threaten coating durability and weatherability. A resin poor coating and rough surface profile promote coating oxidation and embrittlement and encourage the trapping of dirt and fluids that degrade appearance and complicate cleaning. Structural strain encountered in flight can more readily fracture high profile coatings creating opportunities for fluid penetration and corrosion. Experience shows that smooth, resin rich coatings generally clean and weather better than coatings roughened by brittle extender pigments.

2. Concept

The Air Force Research Laboratory has recently focused coating research effort on approaches to durable cleanable low gloss coatings that invoke lowered concentrations of extender pigments. These systems rely on alternative polymer matrix structures to help achieve very low gloss at no expense to other optical properties or key mechanical and thermal properties. The concept utilizes compatibilized immiscible resins to form a phase separated polymer matrix. The discontinuous phase is crosslinked into the continuous matrix creating a thin interface capable of transferring applied stress. The differing refractive indices for the two polymer phases and the size of the included particles create an effective scattering mechanism, lowering gloss. The inherent versatility of the chemistry associated with the multiphase system provides broad opportunity to engineer physical film properties over a significant range through control of the stress carrying ability of the interface. Toughness, barrier properties, radiation resistance, hardness, and elasticity are mainly governed by the choice of resins and additives. Compatibilized blends can unite diverse resin properties to give, in principal, performance beyond that offered by either constituent resin alone[1].

Compatibilization in the present context implies crosslinking throughout the bulk of the incompatible polyols and across their interface. The process is depicted schematically in Figure 1. Blend morphology is largely governed by the relative surface energy of the polyols but is strongly affected by processing. The creation of a thin, stress bearing interface between phases is an important feature of compatabilization. Interface evolution is illustrated in two steps in Figure 1; prior to crosslinking, a physical blend wherein the interaction between phases is Van der Waals forces acting across a large gap and subsequent to crosslinking, covalently bonded phases. The compatibilized immiscible blend is called a polymer alloy. The central parameters for light scattering are the size and shape of the included phase and the difference in refractive index between polymer phases. Light scattering parameters can be systematically varied through choice of the resins and the blend composition. Interfacial bonding may be varied from pure dispersive to covalent through selection of compatabilizer chemistry and reaction index. It remains to be shown through experiment that compatabilization in the sense described in Figure 1 is, in fact, achieved.

ALLOY

Immiscible blend

← d →

compatibilized

Hydrocarbon polyol

- F-C-O-H

H-O-C-H-

Fluoro-
hydrocarbon
polyol

void

+ isocyanate

-OCN-R-NCO-

$$\text{-CO-NH-}$$

$$\text{-F-C-O-C-N-R-N-C-O-C-H}$$
$$\quad\quad\overset{\parallel}{O}\quad\quad\overset{\parallel}{O}$$

H   H

-CO-NH-

-CO-NH-
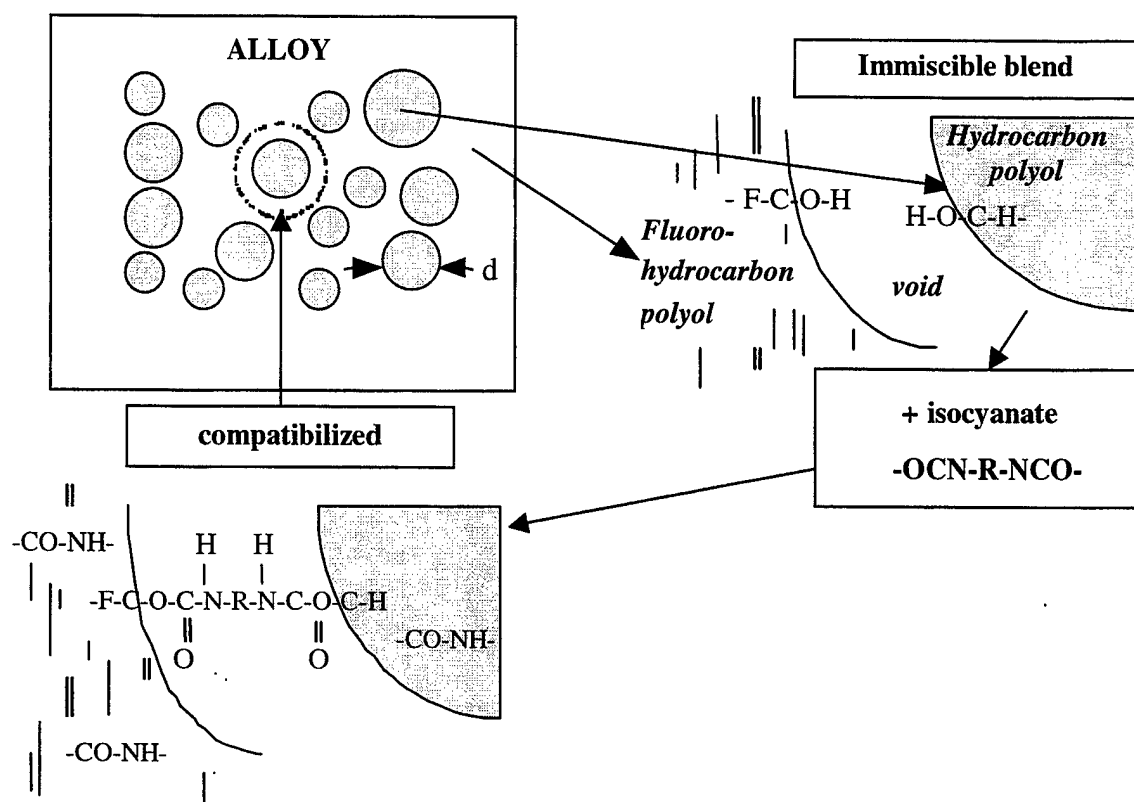
Figure 1. Distinguishing Features of Compatabilization of Two Immiscible Polyols.

The gain in PVC budget that may be anticipated with separated phase systems can be estimated from existing screening test results on developmental polymer alloy topcoat systems[2]. Figure 2 shows the progression of 85^0 gloss from an uncoated, primed, 2024-T3 aluminum substrate to a fully pigmented topcoat meeting a specified color standard. These data[2] correspond to a series of films homologous in fluorohydrocarbon-polyester polyol blend and isocyanate compatabilizer. The 65 unit drop in gloss from the uncoated primed T3 substrate to the same substrate coated with unpigmented polymer alloy indicates the sizeable gloss reduction that can be achieved with a phase separated polymer morphology. Key effectiveness parameters are the difference in polyol surface energy and refractive index.

Figure 2 further shows that prime pigments at a loading sufficient to impart desired color and hiding power exert a minor influence on gloss necessitating the addition of extender pigment to reach the ultra low gloss target region, i.e. gloss < 5. It is significant that the PVC delivering ultra low gloss is low ($\approx$18%) for the polymer alloy system compared to

the traditional topcoat system ($\approx$40% or greater[3]) that is based on a high loading of organic or inorganic extender pigments in a monolithic polymer matrix.

85 degree gloss for FP_PU series from
primed T3 substrate to fully pigmented system
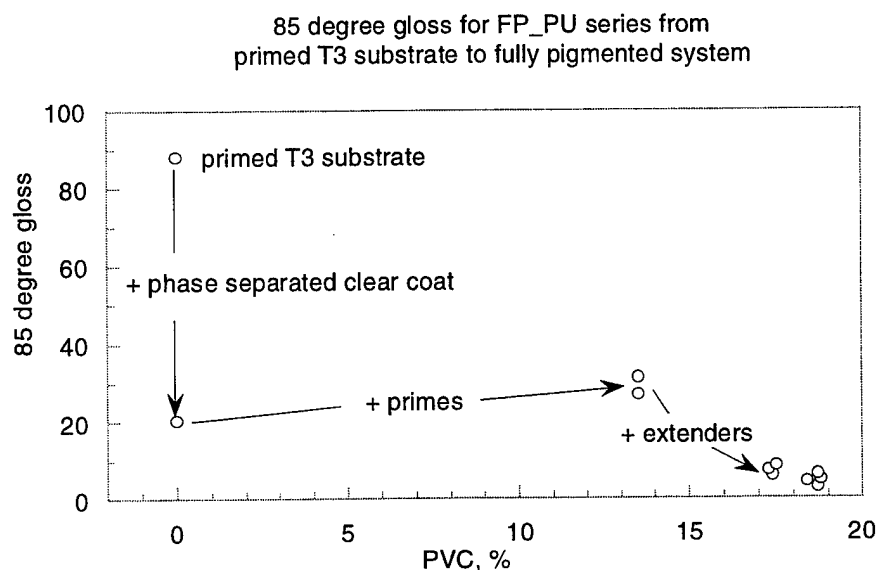
Figure 2. Influence of phase separation and pigmentation on gloss in a homologous series of films. The polymer matrix is a fluorohydrocarbon polyester urethane alloy at 1:1 polyol ratio.

The polymer alloy concept appears to offer broad opportunity to affect properties other than optical near percolation threshold[2,4] (percolation threshold will be synonymous with CPVC for many film properties). As a first illustration, the important mechanical film property of elasticity as gauged through GE Impact[2] is compared with 85[0] gloss in Figures 3A and 3B. Generally the sensitivity of properties to structure fluctuations maximizes near pigment percolation threshold. The region of increased uncertainty in measured property values is delineated by closed dashed curves in Figures 3A and 3B. Data beyond the high noise region show GE Impact falls to the area of 10% simultaneous with gloss reaching ultra low values. The quest is to raise GE Impact to 40% in the ultra low gloss region. The basic question underpinning this quest is: are gloss and elongation linked in an invariant manner through PVC?

The data in Figures 3A and 3B show that elongation varies with PVC similarly to gloss for PVC above primes. In the systems of Figures 2 and 3, primes make up PVC$\approx$13% and extender pigment comprises the increase above 13%. The threshold PVC at which significant decline in properties onset is $\approx$15%, very near primes alone, and ultra low gloss is achieved by $\approx$18%. The additional 3% extender loading is low compared to traditional monolithic polymer matrix systems[3]. The effectiveness of the polymer alloy system suggests that the extender is concentrated in one of the two incompatible polymers comprising the matrix. Preferential segregation of pigment in one phase admits a method for engineering enhanced elongation or other properties such as electronic transport and toughness separate from gloss. However, the data of Figure 3B warn that

achieving a GE Impact of 40% at the PVC giving ultra low gloss will require careful exploitation of all available alloy parameters.

Other polymer alloy coating properties depend in a rather more straightforward manner on composition and morphology. It will be shown, for example, that polymer alloy systems having the fluoropolymer as the continuous phase are hard (1H to 4H) relative to monolithic polyurethane (2B to 1H), and the polymer morphology can be manipulated through selection of polyol ratio. Important film properties such as toughness and surface energy can be manipulated over broad ranges through compositional choices. It will be shown that a hard, tough polymer alloy film favors cleanability and durability.

85 degree gloss for all samples in FP_PU series
FP=L552, PU=polyester polyol, 1:1
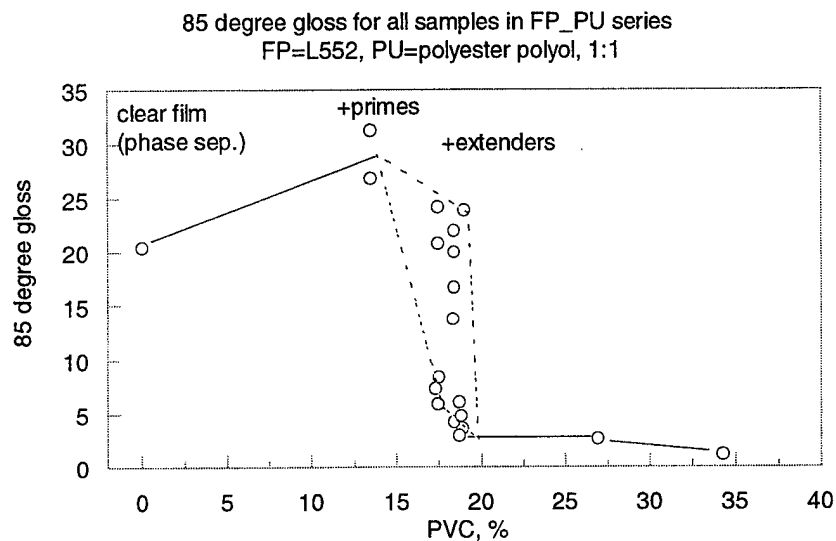
Figure 3A. Variation of gloss with extender pigment loading through percolation threshold.

GE Impact for all samples in FP_PU series
FP=L552, PU=polyester polyol, 1:1
(60%= maximum elongation tested)
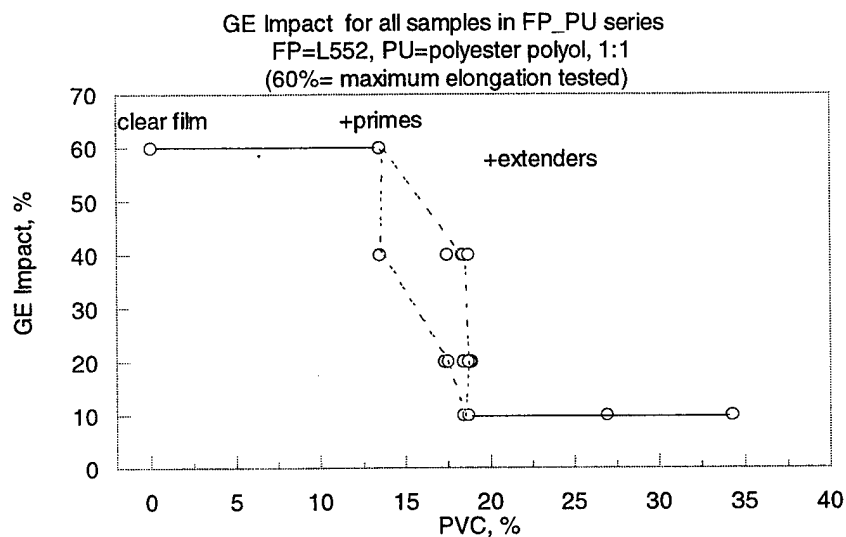
Figure 3B. Behavior of GE Impact through percolation threshold. A sample 'passes' the GE Impact value shown. The maximum elongation produced in the tests was 60%.

3. Scope of Present Work

Clear and pigmented polymer alloy coating systems will be discussed to illustrate application of the concept and to demonstrate the breadth in structure and properties that are inherent to polymer alloy systems. The systems utilize two incompatible polyols selected on the basis of surface energy and index of refraction to insure serious incompatibility and to meet a necessary condition for light scattering. Polymer alloy morphology is elucidated through the study of *clear* films wherein the polyol ratio is systematically varied over the full compositional range to capture phase reversal. *Fully pigmented* topcoat systems are formulated at selected polyol ratios and subjected to a battery of coating screening tests in an aircraft topcoat feasibility study.

4. Experimental

a. Materials for Unpigmented and Pigmented Test Systems

The test films are of two kinds; clear and fully pigmented polymer alloy systems. Two fluorohydrocarbon polyols, one polyester polyol, and one polyisocyanate supply the resins. The fluoro and polyester polyols are seriously incompatible and the isocyanate reacts with both to form in present terminology a fluoro polyester urethane alloy.

Clear films permit investigation of the range in morphology that may be realized through compositional choices. Also, the effects of compatabilization on final film properties may be studied more directly in clear film experiments than with pigmented films containing multiple complex surfaces. The fluoro polyols used in the present experiments are Lumiflon L552 and Lumiflon L200 produced by Asahi Glass Company, Ltd. and marketed in the U.S. by Zeneca Resins. The relevant structural differences between the two polyols cannot be specified in a satisfactory manner on the basis of data made available by Zeneca Resins. The same polyester polyol and aliphatic polyisocyanate were used in all test systems to limit the number of materials variables.

Stated on the basis of solid resin content the clear film compositions investigated include 1:0 (100% fluoro polyol), 3:1 (75% fluoro polyol, 25% polyester polyol), 1:1 (50% fluoro, 50% polyester polyol), 1:3 (25% fluoro, 75% polyester polyol), and 0:1 (100% polyester polyol). It will be shown that the continuous phase in both series of clear films is fluoro urethane through 1:1 and polyester urethane at and beyond 1:3. Samples designations state the fluoro polyol type and the ratio of fluoro to flexible polyester polyol. Hence, 552_1_1, 552-1-1, and 552 1:1 all signify that Lumiflon L552 is combined 50:50 on the basis of resin solids with the polyester polyol. Unless stated otherwise, the NCO:OH index for all systems is 1.60.

The potential worth of a polymer alloy resin matrix as a candidate for an advanced aircraft topcoat can be adequately appraised only by subjecting fully pigmented films to the kinds of evaluations of barrier/corrosion properties, wear/weathering, rain erosion, elasticity, and gloss that are standard to the industry. To this end, pigmented polymer

alloy systems were created to elucidate the influence on film properties from fluoro polyol structure, composition (i.e. fluoro:polyester polyol ratio), and NCO:OH reaction index. The pigmented systems use Lumiflon L552 and Lumiflon L200 at 1:1 and 3:1 to the flexible polyester polyol. A single hard, crystalline, inorganic, extender pigment, Syloid 620, was used to adjust gloss to requisite values. A small addition (three weight percent on total pigment solids) of the fluoroparticle, Fluo HT-LS (Micro Powders, Inc.), was incorporated to enhance radiation resistance, lower the coefficient of surface friction, and to aid spray application. One pigmented system was selected for extensive characterization by a third party to further explore performance limits.

Formulation parameters that are critical to topcoat performance and that were examined in our experimental matrix include: (1) the fluoro:polyester polyol ratio, because its value determines the morphology of the polymer matrix and hence a number of film properties, (2) the NCO:OH reaction index, since this index governs the ratio of urea-to-urethane linkages realized in the final film which influence attributes such as chemical resistance, toughness, and elasticity and, (3) the ratio of pigment volume to total solids volume (PVC), because PVC relative to CPVC effectively governs the involvement of the polymer matrix. Other formulation parameters that were varied to manipulate matrix morphology, pigment dispersion, and application parameters like dry-to-touch, dry-to-tape, wet edge, and pot life included surfactants, solvents, milling, and catalyst chemistry and level[2-4].

b. Analytical Methods

Clear film structure at the micrometer scale was characterized by optical and IR microscopies and light scattering measurements. Physical properties measurements for clear and pigmented films include (complex) modulus and structural transition maps obtained from Dynamic Mechanical Analysis (DMA) of free standing thin films, and conventional coatings tests that manifest mixed aspects of complex properties like hardness, toughness and wear. A basis is sought for correlating film performance with morphology.

c. Physical Properties

1. Clear Film Gloss and Hardness

Clear films were formulated at three ratios of fluoro polyol to polyester polyol. The polyester is branched and the polyisocyanate is a trimer isocyanurate ring.

Films were cast on glass substrates to aid visualization of the effect of polyol structure on optical clarity. Film hardness was appraised through pencil hardness. The solvent cast films were air dried for 24 hours followed by an oven cure of 48 hours at 125 ^{0}F. Results are given in Table 1 that is taken from Reference 2.

Table 1. Hardness and Optical Clarity of Fluoro Polyester Urethane Alloys

Sample[1] & test	0:1[2]	1:3[2]	1:1[2]	3:1[2]	1:0[2]
L552/polyester					
pencil hardness	<2B	<2B	HB	F-H	H
film clarity	clear	cloudy	cloudy	cloudy	clear
NCO:OH index[3]	1.10	1.30	1.58	2.01	2.75
L200/polyester					
pencil hardness	~	2B	HB	H	H
film clarity	~	cloudy	cloudy	cloudy	clear
NCO:OH index	~	1.18	1.30	1.49	1.83

1. The fluoro polyols are Zeneca Lumiflon 552, and Lumiflon 200.
2. x:y gives the ratio of fluoro to polyester polyols.
3. NCO:OH indicates the ratio of NCO to OH

The clear film data in Table 1 reveal two important features of fluoro polyester urethane alloys. First, the end points show that the intrinsic pencil hardness of 100% polyester urethane on a glass substrate is modest, about 2B, while both the 100% fluoro urethanes exhibit an intrinsic hardness four units greater (H). The hardness of the three alloy compositions varies between these limits, presumably according to the polymer that constitutes the continuous phase. The data are consistent with a polyester urethane continuous phase at 0:1 and 1:3 with phase inversion to a fluoro urethane continuous phase occurring by 1:1.

Second, the optical clarity indicates that the fluoro and polyester polyols are incompatible in the solvent system employed. Visual inspection suggests the morphology of the dry film can be described in a first approximation as an included phase comprised of small more or less spherical particles dispersed throughout a continuous phase (a more exact description is developed subsequently). The polyol incompatibility responsible for clouding the film reduces gloss through light scattering at the film surface and internally at the interface of the included polymer particle with the continuous matrix polymer of differing refractive index. Homopolymer data suggest the difference in refractive index may reach 0.2.

In summary, clear film experiments demonstrate an ability to control polymer matrix morphology at the micrometer scale simply through the mass ratio of the incompatible polyols. This easy artifice offers an efficient method for engineering a number of optical and mechanical properties since the gloss reduction afforded by phase separation reduces the concentration of extender pigment needed to realize ultra low gloss. The continuous phase will govern important surface parameters like surface energy.

2. Morphology of Clear Films by Vibrational Spectroscopy

a. Scope of IR Measurements

The series 200 and 552 polymer blends were characterized by Raman, conventional- and synchrotron-IR microscopy. These three techniques provide full spectral analysis of the vibrational region with good spatial resolution. The capabilities of these techniques are summarized in Table 2.

Table 2: Comparison of Technique Capabilities

Technique	IR-Microscopy	Synchrotron IR Microscopy	Raman Microscopy
excitation source	tungsten glow-bar	synchrotron	514 nm Ar+ laser
spectral region	400-5000 cm^{-1}	600-5000 cm^{-1}	100-5000 cm^{-1}
spatial resolution	20 μm	2-10 μm	0.1 μm
spectral resolution	4 cm^{-1}	4 cm^{-1}	2 cm^{-1}

The use of high spatial resolution techniques allowed the interrogation of well-defined areas within the multi-component polymer matrix. High resolution IR microscopy is made possible by the use of synchrotron radiation in the mid-infrared region as the infrared source for the spectrometer. Synchrotron radiation provides a source brightness approximately 1000 times higher than a conventional glow-bar source. The enhanced brightness allows the use of very small apertures and thus high spatial resolution analysis of the sample. This recently developed technique has been applied in a variety of research areas including cell biology, semiconductor analysis, coatings analysis and forensics[5]. In the present research, the synchrotron source enabled the analysis of relatively thick samples with a small aperture. Spatial resolution is improved by an order of magnitude over that of conventional microscopy.

A large number of vibrational studies on crosslinked polyurethane coatings are reported in the literature. Depth profiling investigations[6,7], photooxidation studies[8] and a general review[9] are invoked to confirm assignments proposed in this work. Fewer studies of fluoropolymer systems are available, although results for poly(vinylidene fluoride)[10,11] are used to support our assignments. Finally, standard reference materials aided vibrational assignment[12-16].

b. Experimental

Vibrational analysis was carried out on solvent cast films drawn down on glass substrates. Free standing films for analysis were lifted from the glass. The polyol and isocyanate resins are described in Section 4a. In all cases, the NCO:OH ratio was 1.60 and the film thickness was approximately 30 microns. Conventional IR microscopy was performed on a Spectra-tech IR Research Plan microscope coupled to a Nicolet Impact 410 spectrometer. The detector was a liquid nitrogen cooled MCT. A fixed 1.5 mm

round aperture was used to isolate a 100 micron spot at the sample. Spectra were acquired in transmission mode using 100 co-added scans and a 4 cm^{-1} spectral resolution. Samples were rolled onto 2mm KBr plates. The KBr plate was used as the sample background.

High spatial resolution IR was carried out on a Nic-plan microscope with a liquid nitrogen cooled MCT detector coupled to a Nicolet Magna 670 spectrometer. A computer controlled stage was used to produce line maps. A 100 micron pinhole formed the top and bottom apertures in transmission mode resulting in a 10 micron spot at the sample. Samples were rolled onto 2mm KBr plates. Typically 200 scans were co-added at each point with a 4 cm^{-1} spectral resolution. The KBr plate was used as the sample background.

Raman micro-spectra were acquired on a Renishaw 2000 spectrometer using a 514 nm argon ion laser as the excitation source. Raman emission was collected in a 180 degree geometry using a 50x glass microscope objective. The excitation spot limited the spatial resolution to less than 0.1 micron and no additional apertures were used. Laser power at the sample is estimated to be 150 milliwatts.

c. Results

A study of the individual components was undertaken to further understanding of the chemical and physical characteristics of the polymer alloys. The homopolymer study is reported in Appendix A. The blends study is presented here.

Polymer Alloys

The range of polymer compositions examined in infrared and Raman microscopy are summarized in Table 3 along with the general morphological features that were found to distinguish each composition. The summary is followed by detailed discussion of the individual blends.

Table 3: Polymer Alloy Summary

Blend	Series 200	Series 552
1:0	clear film	clear film
3:1	cloudy homogeneous film	cloudy homogeneous film
1:1	regular spherical, polyester urethane inclusions in fluoro urethane matrix	regular spherical, polyester urethane inclusions in fluoro urethane matrix
1:3	irregular fluoro urethane inclusions in polyester urethane matrix	spherical, fluoro urethane inclusions in polyester urethane matrix
0:1	clear film	clear film

<u>Series 200 1:1</u>

The polymer alloy produced from equal mixtures (on the basis of resin solids) of Lumiflon 200 fluoro polyol and Desmophen 670A-80 polyester polyol crosslinked with an HDI adduct results in a film of regular, spherical inclusions evenly distributed in a continuous phase. A typical micrograph is shown in Figure 4. This film was investigated using both Raman and infrared micro-spectroscopy. The infrared and Raman spectra taken in the continuous matrix and discreet inclusions evident in Figure 4 are shown in Figure 5 and 6. Both the Raman (Figure 6) and IR (Figure 5) spectra demonstrate that the continuous phase is primarily made up of fluoro urethane derived from the Lumiflon while the inclusions are almost pure polyester urethane derived from the Desmophen. This conclusion can be understood by comparing the similarities between the spectra of the pure components included in the figures with the spectra of the continuous and discreet phases of the polymer alloy. Some particular bands to consider are the C-F stretching bands at 1120 cm^{-1} (IR) and 1025 cm^{-1} (R), and the two pairs of C-O related bands at 1165, 1137 cm^{-1} and 1095, 1075 cm^{-1} (IR) which identify the Lumiflon and Desmophen structures, respectively.

It is also evident that the spectra indicate a certain degree of mixing of the two components. This is most obvious in the bands of the carbonyl region (1620-1800 cm^{-1}) in both the Raman and the infrared. In the Raman, the pure Lumiflon fluoro urethane contains only a single carbonyl band assigned to the HDI crosslinking agent at 1758 cm^{-1}. However the spectrum of the continuous phase of the polymer alloy shows a second carbonyl band at 1722 cm^{-1} that is due to the ester linkages of the Desmophen and is not observed at all in the pure fluoro urethane. This effect can also be observed in the infrared spectra although the carbonyl region is more complicated due to the appearance of a carbonyl band indicative of the Lumiflon urethane linkages at 1692 cm^{-1}.

The origin of this mixing is difficult to ascertain. It is not likely to be due to insufficient spatial resolution as the spatial resolution of both the synchrotron IR and the Raman are well above the observed size of either of the phase domains. Another possible explanation for the spectral mixing is that the continuous phase completely encloses the inclusions. This would explain why there are components of the continuous phase observed in the spectra of the discontinuous phase but not the reverse. Similarly, it may be possible that the film production process results in a skin or laminate type structure being produced of the discontinuous phase on top of the continuous phase. However, this seems unlikely as there are no other indications of this phenomenon. Furthermore, the depth penetration of visible excitation Raman spectroscopy is very shallow and could be expected to detect such a skin. Finally, phase separation may produce a range of included particle sizes below the level resolved in the present measurements. This sort of 'mixing' could benefit the properties of the polymer alloy as it would improve film isotropy.
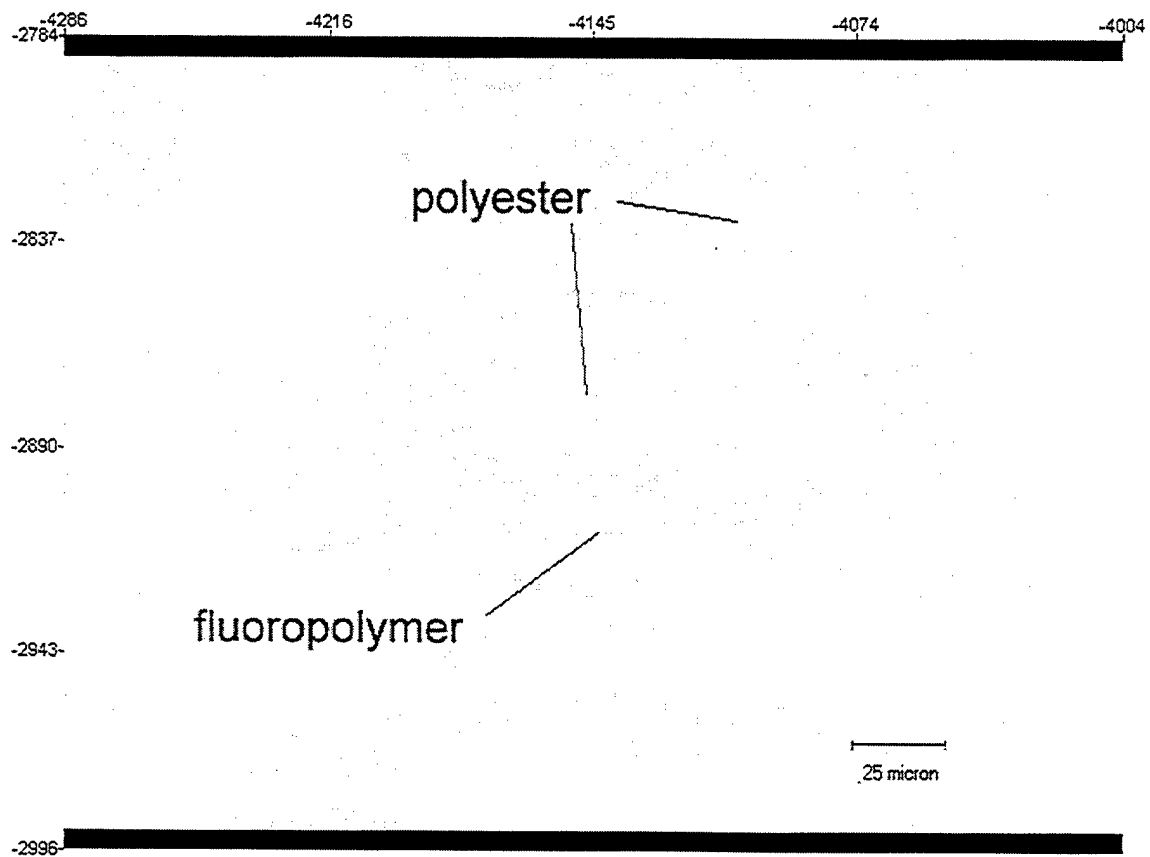
Figure 4. Micrograph of series 200 1-1 alloy, equal amounts of L200 and D670.
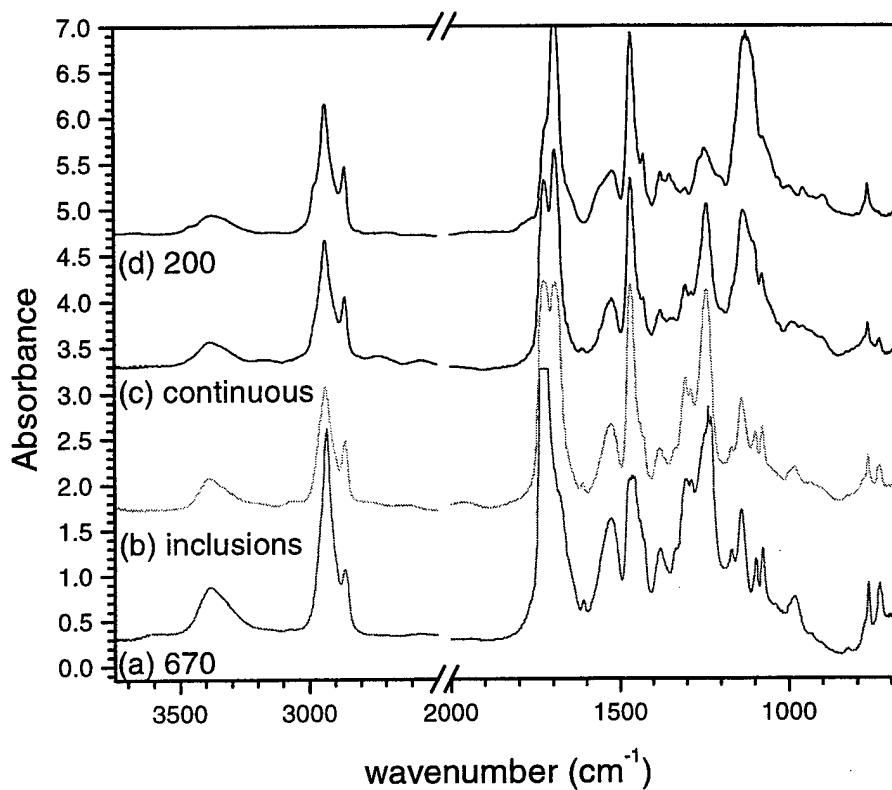
Figure 5. IR spectra of series 200-1-1 alloy (a) pure D670, (b) included phase containing D670, (c) continuous phase containing L200 and (d) pure L200.
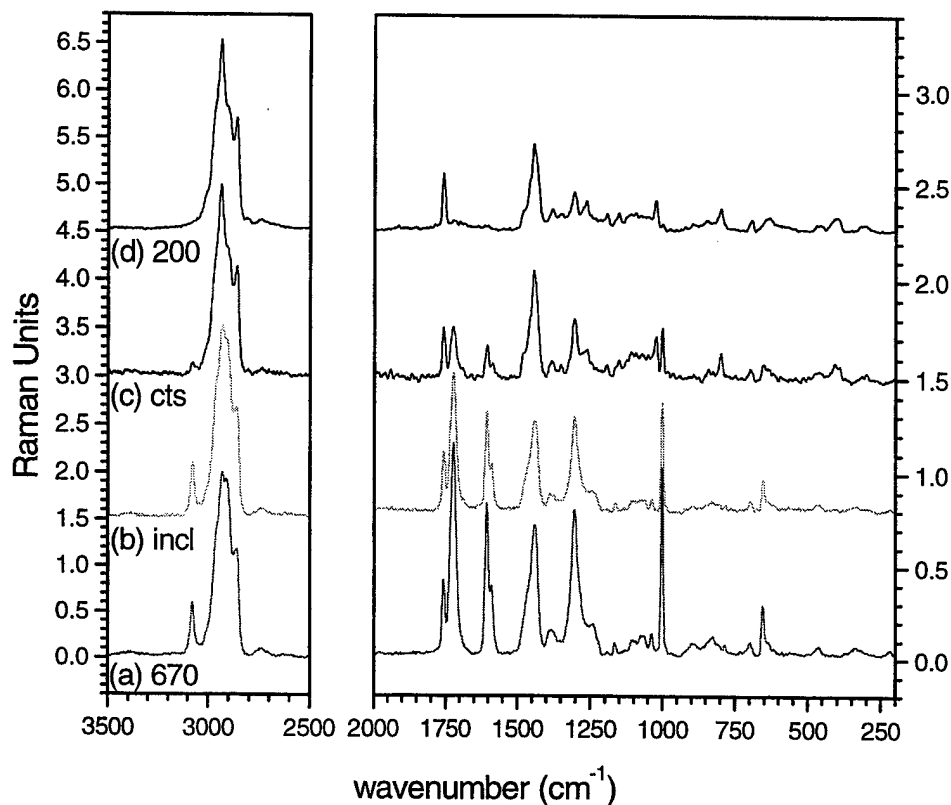
Figure 6. Raman spectra of series 200-1-1 alloy (a) pure D670, (b) included phase containing D670, (c) continuous phase containing L200 and (d) pure L200.

Series 200 3:1

A visual examination of the 3:1 polymer alloy reveals no resolvable individual phases in the uniformly cloudy film. The material is translucent compared to the water white films cast from either pure component. Infrared and Raman analyses carried out on the 200 3:1 alloy film are given in Figures 7 and 8. The infrared spectrum of the 3:1 blend contains two C=O bands at 1721 and 1692 cm^{-1}, the C-O ester related peak at 1239 cm^{-1} and the C-F band at 1120 cm^{-1}. Similarly, the Raman contains bands due to the aromatic components of the Desmophen (1606, 1589 cm^{-1}), the Lumiflon C-F band at 1025, and two carbonyl peaks at 1758 and 1723 cm^{-1}. Both spectra indicate that both components are present in the film and they appear to be evenly distributed throughout the film. Based on the relative Raman intensities of the aromatic peaks and the carbonyl bands, an estimate of the relative composition of the system indicates that the entire film is very similar in composition to the continuous phase of the Series 200 1:1 blend.

These results support the hypothesis that the continuous phase is actually a mixture of fluoro urethane and polyester urethane in the form of an energetically preferred blend. In the case of the 1:1 polymer alloy, the polyester phase separates out of the continuous phase to form discreet domains of a size that is discernible to the human eye, whereas in 3:1 the domain size is below the resolution of the microscope.

Figure 7. IR spectra of series 200-3-1 alloy (a) pure D670, (b) unresolved 3-1 mixture, and (c) pure L200.
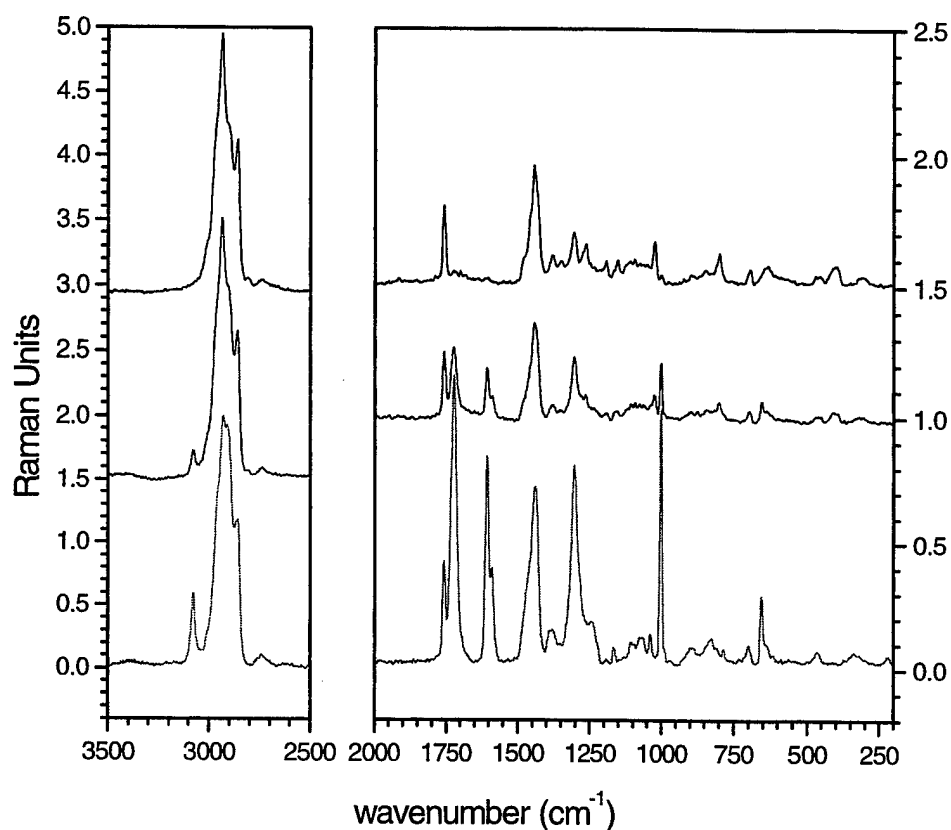
Figure 8. Raman spectra of series 200-3-1 alloy (a) pure D670, (b) unresolved 3-1 mixture and (c) pure L200.

Series 200 1:3

A photomicrograph of the 1:3 polymer alloy is given in Figure 9. This composition produces a very different morphology from that observed for the 1:1 polymer alloy. The inclusions in 200-1-3 are larger, irregular and unevenly distributed throughout the film. There are also domains within the inclusions that could be gas bubbles or continuous phase material trapped within the inclusion. It was not possible to isolate these small regions for spectroscopic investigation.

18

The infrared and Raman microscopic analyses are shown in Figures 10 and 11. As expected for such a large excess of polyester, the Desmophen polyester urethane forms the continuous phase. This dominance is indicated by the familiar aromatic stretches (1606, 1589 cm^{-1}) as well as the strong polyester carbonyl band (1722 cm^{-1}) in the Raman spectrum. The C-O related stretching bands at 1165, 1137, 1095 and 1075 cm^{-1} in the infrared spectrum also support this identification. The large inclusions contain the Lumiflon fluoro urethane as indicated by the C-F stretches at 1025 cm^{-1} (R) and 1120 cm^{-1} (IR). The aromatic, carbonyl and C-O peaks in the inclusions spectra indicate some mixing of the Desmophen and Lumiflon urethanes. The mixing is similar to the mixing witnessed in the predominantly fluoro urethane phase of the other blends but is higher in polyester content. The 200 1:3 formula favors higher polyester urethane and the unresolved small inclusions within the fluoro urethane included phase may be pure polyester urethane.
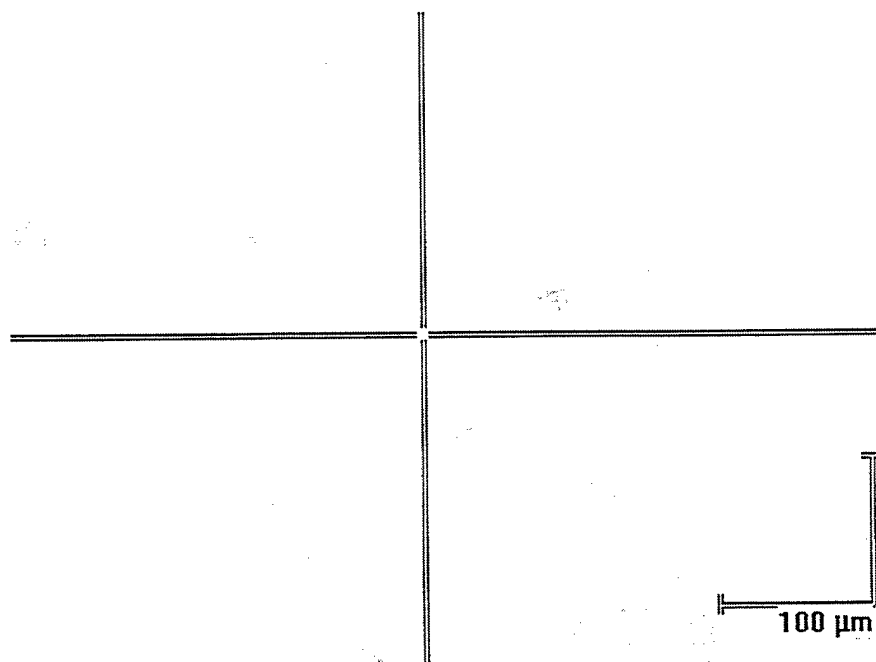
Figure 9. Micrograph of series 200 1-3 alloy.
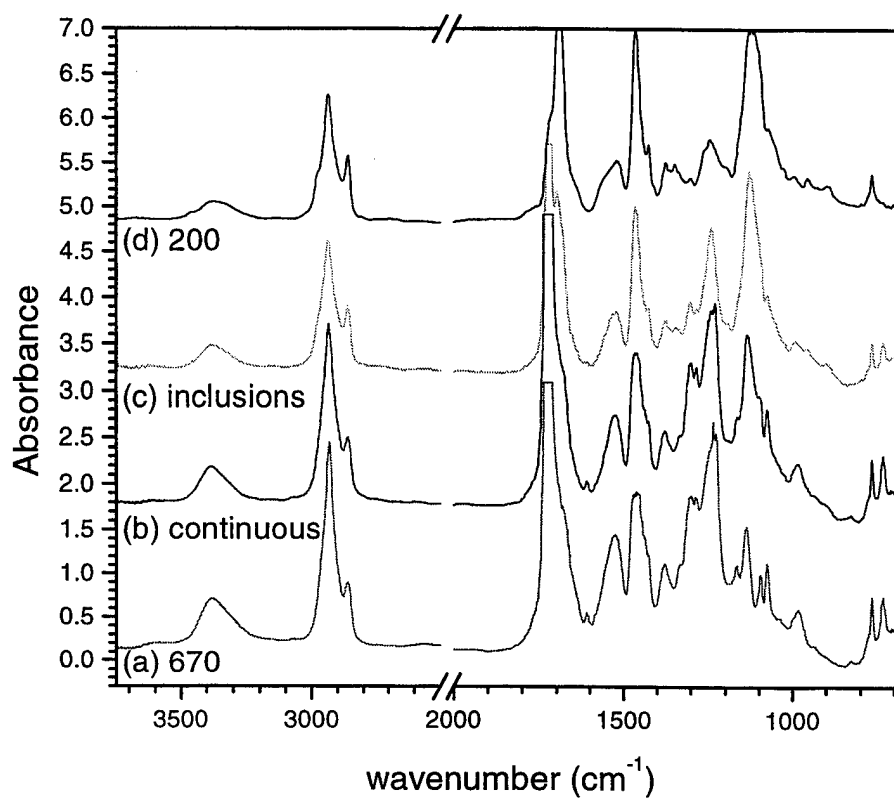
Figure 10. IR spectra of series 200-1-3 alloy (a) pure D670, (b) continuous phase containing D670, (c) included phase containing L200 and (d) pure L200.
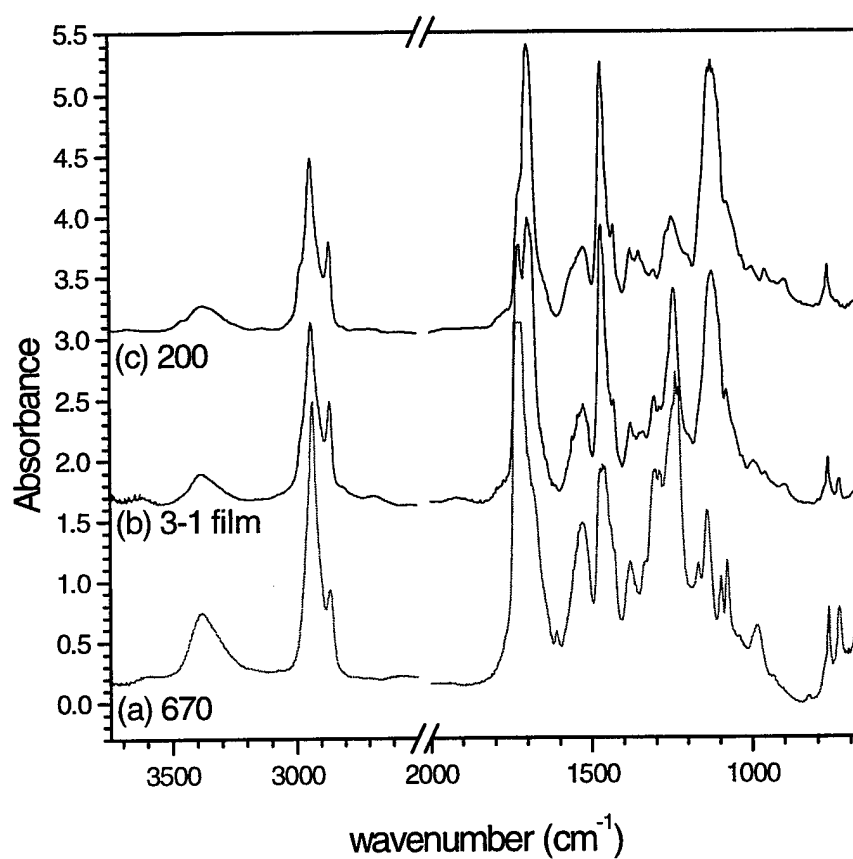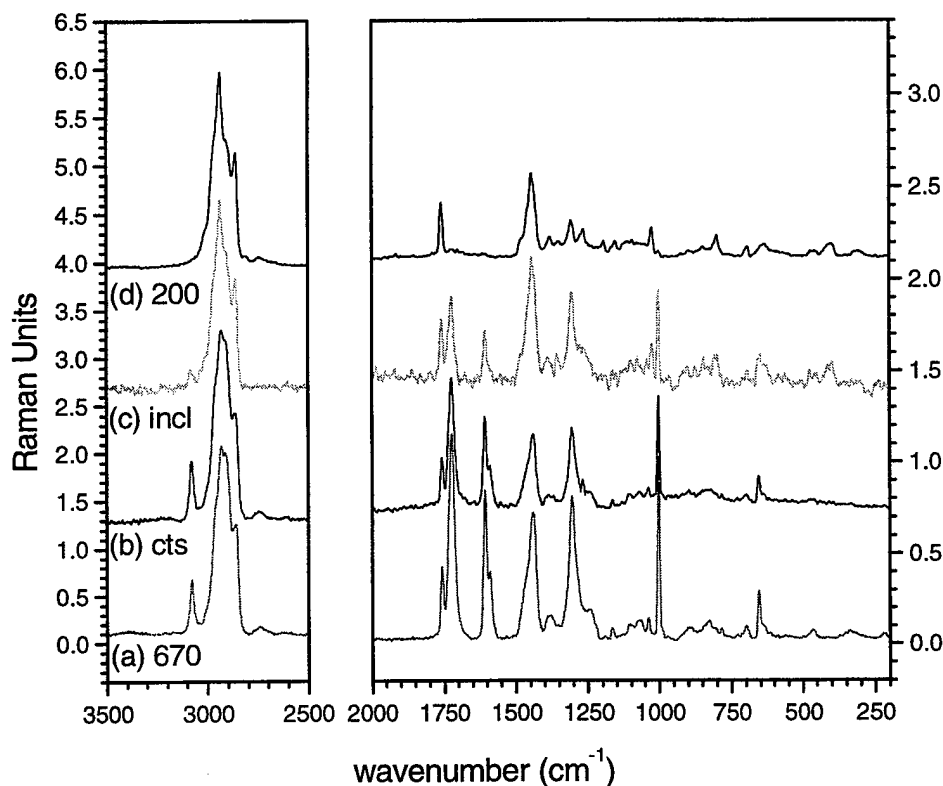
Figure 11. Raman spectra of series 200-1-3 alloy (a) pure D670, (b) continuous phase containing D670, (c) included phase containing L200 and (d) pure L200.

Series 552 1:1

The Series 552 1:1 polymer alloy results in a film with many regular, spherical inclusions imbedded in a hazy continuous phase. Raman and infrared micro-spectroscopy identify the inclusions as Desmophen polyester urethane and the continuous phase as a mixture of Desmophen urethane and Lumiflon 552 fluoro urethane. The mix in the continuous phase is similar to that observed for the Series 200 1:1 alloy and suggests that the Lumiflon 552 and Desmophen phase separate until a particular energetically favorable composition obtains. Phase separation can occur on any spatial scale. A range of included polyester urethane particle sizes extending below the level resolved would account for the haze.

Series 552 1:3

This polymer alloy produces micrographs visually similar to those for the Series 552 1:1 alloy. The size and spatial distributions of the inclusions are a little less regular than

observed for the 1:1 alloy. However, the inclusions are still spherical and the size range is not nearly as wide as that observed for the Series 200 1:3 alloy. The spectroscopic study of 552 1:3 identifies the continuous phase as Desmophen polyester urethane. The included phase shows substantial mixing of the Desmophen and Lumiflon 552 urethanes similarly to the Series 200 1:3 system. The mixing is most obvious in the appearance of the carbonyl band at 1723 cm^{-1} and the aromatic stretches at 1607 and 1585 cm^{-1} (R). As Lumiflon 552 is a poor scatterer, it is difficult to quantify the mix comprising the included phase.

Series 552 3:1

Just as with the Series 200 3:1 alloy, the 552 3:1 polymer alloy does not phase separate into visually resolvable inclusions. The Raman and infrared spectra contain bands due to both the Lumiflon 552 and the Desmophen urethanes. These include the carbonyl band (1723 cm^{-1}, R) and the aromatic bands (1606, 1587 cm^{-1}, R) of the Desmophen as well as the C-F stretches (1349 and 1122 cm^{-1}, IR) of the Lumiflon 552 urethane. An estimate based on relative peak intensities of the two components places the mixing close to that in the continuous phase of Series 552 1:1.

d. Compatabilization

An important feature of polymer alloy systems for application in coating systems is their potential for compatabilization, that is the formation of urethane linkages across the phase interface. Infrared and Raman microscopy were used to investigate the chemical structure of the interface in selected blends of Table 3.

Infrared spectral line maps having a spatial resolution of 10 microns were acquired across the interface. The quantity of interest is the variation in the normalized band intensities specific to the Lumiflon, Desmophen and HDI structures with position relative to the interface between the discreet and continuous phases. The moiety concentrations associated with the selected band intensities are shown in Figure 12 for the 200 1:1 polymer alloy. Figure 12 shows the Desmophen and Lumiflon urethane concentrations varying inversely to one another consistent with our previous analysis of continuous and discreet phase compositions while the HDI concentration is nearly invariant across the interface.

An HDI concentration in quantitative proportion to the polyol hydroxyl concentration would signal an effective, uniformly dispersed compatabilizing agent. It is difficult to interpret the IR signal precisely in these terms because of unresolved phase mixing, over indexing, and unavoidable signal mixing from the two pure phases at their curved interface. We take the slowly varying HDI concentration in Figure 12 as an indicator of a dispersion that has generated the full number of urethane linkages prescribed by the polyol hydroxyl content uniformly throughout the film. This result validates the essential features of polymer alloy formation as depicted in the schematic of Figure 1.
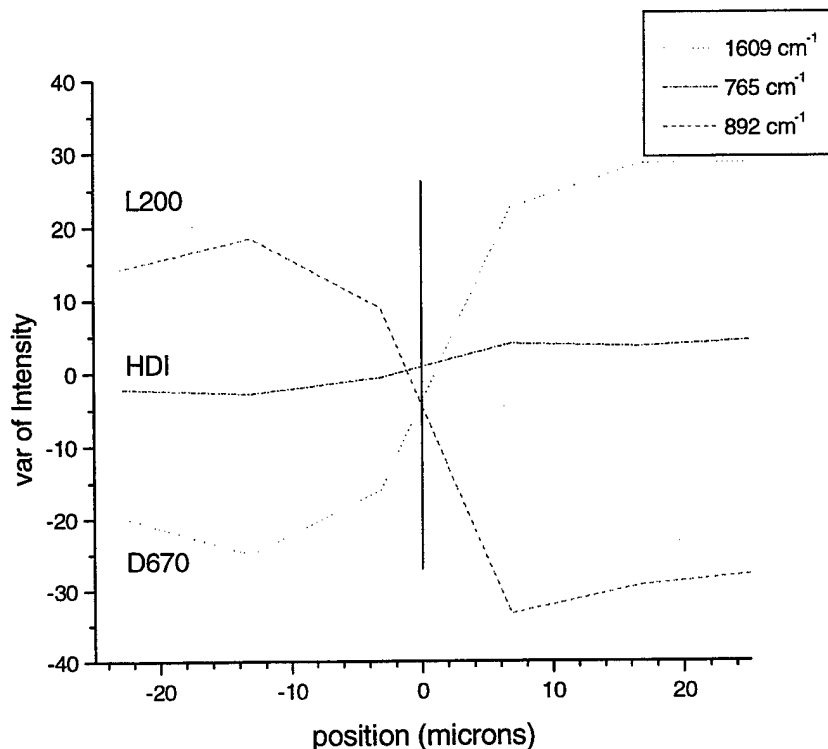
Figure 12. Variation in intensity of bands characteristic for the three components of the series 200 1-1 alloy in a spectral line map across the interface (at 0 microns) from the continuous to the included phase.

e. Conclusions

Vibrational micro-spectroscopy was used to characterize films formed in two series of polymer alloys distinguished by the fluoro polyol. The results show that film morphology including the identity of the phases and the size distribution of the inclusions is dependent on the film composition as defined by the polyol ratio. Overall, an equal polyester polyol and fluoro polyol ratio appears to provide the most regular film for both the 552 and 200 series of polymer alloys. In both cases, the discontinuous phase was found to be composed of the Desmophen polyester urethane while the continuous phase was a mixture of both Desmophen polyester and Lumiflon fluoro urethanes. A study of the chemical structure of the interface prevalent in the Lumiflon 200 system indicated that the HDI curing agent is evenly distributed across the phases. Although it is difficult to account quantitatively for phase mixing and signal mixing arising from the curved interface, this result supports the main features of the proposed compatibilized interface described in the beginning of this work.

3. Morphology of Clear Films by Light Scattering

a. Introduction and Scope of the Measurements

Light scattering measurements in the form of a bidirectional reflectance distribution function (BRDF) can elucidate the functional relationship existing between the gloss of the polymer alloy coating and the index of refraction and size distribution of the included polymer phase particles. If known in sufficient detail this functional can be used to prescribe a size distribution for the polymer inclusions that will maximize internal light scattering. The size distribution parameters define a rather specific target for formulation because maximum scattering of visible light will minimize the loading of extender pigment needed to attain ultra low gloss, and minimum pigmentation works to optimize coating performance. Light scattering measurements performed on unpigmented alloy films towards this goal are described in this Section.

Light scattering is the result of the interaction between an electromagnetic wave and matter, and there are numerous articles and books that survey the types of scattering relevant to immiscible polymer blends[17-21]. Nonlinear scattering mechanisms such as Raman, stimulated Raman, and Coherent Anti-Stokes Raman scattering are not relevant. In most cases, light scattering can be modeled as an interaction between an electromagnetic wave and an electric dipole, either atomic or molecular. This interaction can be modeled on the atomic, molecular or bulk material level. Scattering behavior is also dependent on many variables including source properties such as wavelength, spatial and temporal coherence, and material properties such as index of refraction, absorption (extinction coefficient), and particle size. The index of refraction and absorption coefficient can be given in terms of the permittivity and permeability of the material.

Current models of the relationship of light scattering to structure are largely limited to single scattering events or particle sizes $\ll \lambda$. For clean, smooth, reflective surfaces, there is a linear relationship between the distribution of scattered light and the Fourier transform of the surface roughness[17]. Multiple scattering events such occur in immiscible blends are generally modeled emperically[22,23]. Still, it is logical to assume that the scattering behavior is related to the three-dimensional Fourier transform of the volume discontinuities in the film. On this basis the distribution of sizes and shapes produced by the mixing of resins can be expected to exert a significant influence on the scattering properties of the material.

An experimental method for characterizing the functional relationship between film structure and scattered power will be described and applied to the fluoro polyester urethane alloys with the objective of identifying specific features of the size distribution of the included phase that promote scattering. It will be shown that the complex structure of the blends requires experimental effort beyond the scope of the present study to separate the influence of the surface and bulk structures on light scattering. Present data are sufficient to correlate a salient feature of alloy structure with qualitative trends in

scattering power and so demonstrate the efficacy of the method as an aid to materials design.

b. Bidirectional Scattering Experiment

The scattering properties of materials are evaluated by measuring their bidirectional reflectance distribution function (BRDF). The BRDF is a differential quantity defined as the ratio of the radiance to the irradiance. Both terms are functions of azimuth, elevation and polarization. In practical terms, the bidirectional reflectance distribution function, f, is defined by four parameters--scatter power, P_s, incident power, P_i, receiver solid angle, Ω, and receiver elevation angle, Θ_s, as follows:

$$f = P_s / [P_i \Omega \cos(\Theta_s)]$$

Our capability to measure laser bidirectional scattering resides in two TMA scatterometers; the commercial CASI in-plane instrument and a custom hemispherical laser scatterometer that was uniquely specified to meet the long-range needs of the Air Force and serve as a reference instrument for data and materials generated by other programs. A summary of our laser-scatterometer capabilities is presented in Table 4. The experimental method is described in Appendix B.

Table 4. Table of Laser Scatterometer Capabilities at the OMF

Capability	TMA CASI Laser Scatterometer	TMA Hemispherical Laser Scatterometer
Wavelength	0.544, 0.6328, 3.39, and 10.6 µm	0.325, 0.6328, 1.06, 3.39, and 10.6 µm
Angle of Incidence	$0 - 85^0$	$0 - 89^0$
Angle of Reflection	$0 - 88^0$ (less $\pm 6^0$ at incident angle)	$0 - 89^0$ (less $\pm 1.5^0$ at incident angle)
Polarization	s-Polarized source Unpolarized receiver	Linear (s, p, or variable) in both source and receiver
Sample Temperature	Ambient	- 65 C to 204 C (- 90 to 400 °F)

c. Scattering Measurement Data

This Section presents the polarized BRDF of resin systems 552, L552 and L200. The L552 and L200 designations refer to the Lumiflon fluoro polyols described previously in Section 4 a. A 552 designation is also used to refer to a set of films nominally the same in composition as the L552 series but nevertheless exhibiting some interesting differences in

scattering properties. Scattering data were collected at an angle of incidence of 60^0. The charts presented in this section illustrate the BRDF vs. the receiver angle. As a point of reference, a receiver at an angle of 60^0 is located in the specular direction of the incident radiation. A receiver at an angle of -60^0 is located in the incident direction. Therefore, large peaks at 60^0 indicate that the sample is specular and does not scatter radiation efficiently. As an additional point of reference, a perfectly diffuse material (Lambertian) has a constant polarized BRDF vs. receiver angle of $1/2\pi$ and an unpolarized BRDF vs. receiver angle of $1/\pi$. Also included in this section are transmission light microphotographs of mixed resin systems illustrating the structure that promotes diffuse scatter.

The first immiscible blend to be discussed is the system 552. The film identification sequence employed states the fluoro and polyester (solids) polyol content. Transmission light photomicrographs of film samples 552_1_1 (50% fluoro, 50% polyester polyol) and 552_1_3 (25% fluoro, 75% polyester polyol) are given in Figure 13 and 14, respectively. The discontinuous features in the morphology evident in Figures 13 and 14 were not apparent at the same magnification in film samples 552_0_1 (100% polyester urethane), 552_1_0 (100% fluoro urethane) and 552_3_1 (75% fluoro, 25% polyester polyol).

Polarized and unpolarized BRDF for 552_3_1, 552_1_1, and 552_1_3 are given in Figures 15, 16, and 17. A comparative summary of unploraized BRDF for the entire 552 series of two parent homopolymers and three blends is given in Figure 18. The BRDF comparison in Figure 18 clearly shows the strong specular reflection for the water white parent homopolymers. Gloss reduction similar to the ~70 unit decrease shown in Figure 2 accompanies the reduction in the specular peak from the two homopolymer films to all three polymer alloy films of Figure 18. Nevertheless, the magnitude of the BRDF and its shape near specular reflection (60^0) indicate the most efficient scatterer of the three polymer alloy morphologies to be 552_1_3.

Generally, a significant difference between the cross-polarized BRDF (the sp and ps curves in Figures 15-17) and the polarized BRDF (ss and pp in Figures 15-17) indicates that the source of scattering is primarily roughness at the geometric surface of the film rather than volume discontinuities internal to the film. Volume scatter generally rotates the polarization state of the incident radiation. For example, samples that exhibit large volume scattering such as Spectralon™ show a crossed polarized BRDF of the same order of magnitude as the polarized BRDF. However, the dependence of the BRDF on polarization observed for the present polymer alloy films might also be connected with the size of the discreet included phase particles being similar to the film thickness thereby limiting the number of multiple internal scattering events and consequently the polarization rotation. Further work is required to separately identify the contribution to scattering from surface and bulk features of the polymer alloy films.

Photomicrographs and BRDF for systems L552 and L200 are given in Figures 19-24. The magnitude of the BRDF and the relative reduction in the specular scattering component identify L552_1_1 as the best scatterer within the L552 and L200 series of films. No member of these two series reduces the specular component (60^0) as well as system

26

552_1_3 discussed previously even though the transmission microphotographs indicate a similar morphology for L552_1_1 and 552_1_3. Closer examination suggests, however, that while the size distribution of the inclusions appears similar for these nominally identical films, the inclusion density is greater in 552_1_3. Apparently, this subtlety is introduced by processing.

The distribution of discontinuities, or inclusions, for sample 552_1_3 was measured manually from photomicrographs. The results are presented in Figure 25. More precise measures of differences in the inclusion size distributions and area densities for the various alloy compositions can be obtained from two dimensional Fourier transforms of the photomicrograph images.

0.5 mm
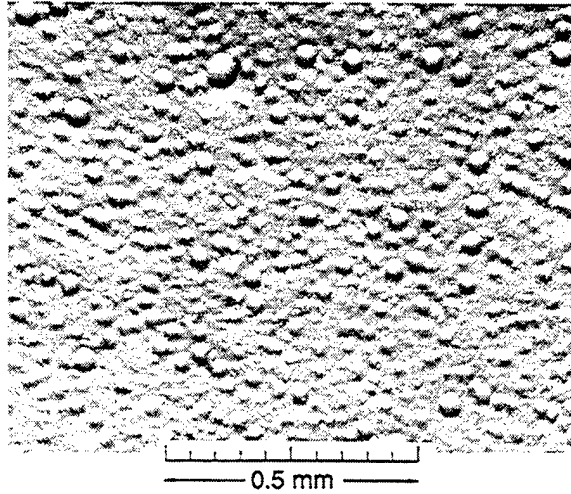
Figure 13. Light transmission photomicrograph of sample 552_1_1.

0.5 mm
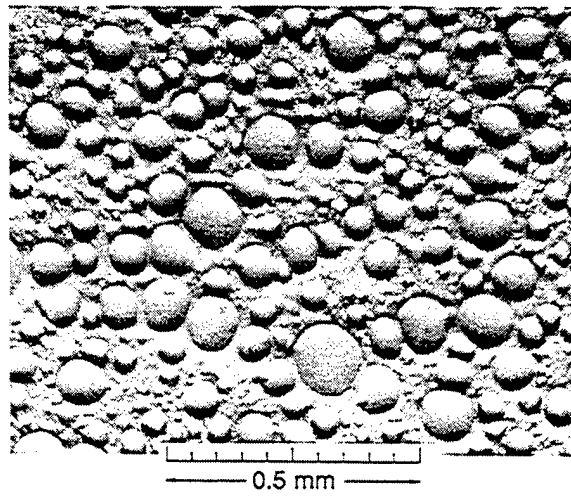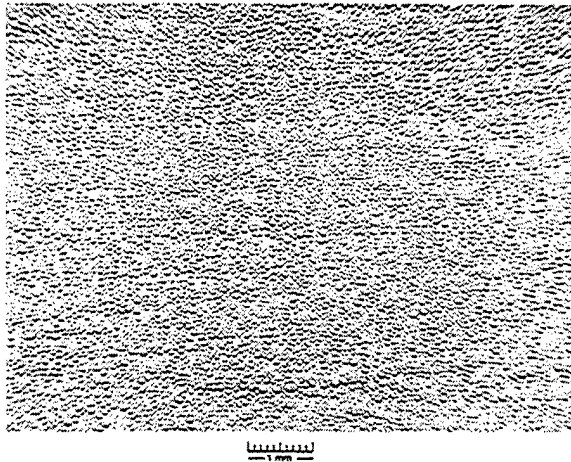
Figure 14. Light transmission photomicrograph of sample 552_1_3 at two magnifications.
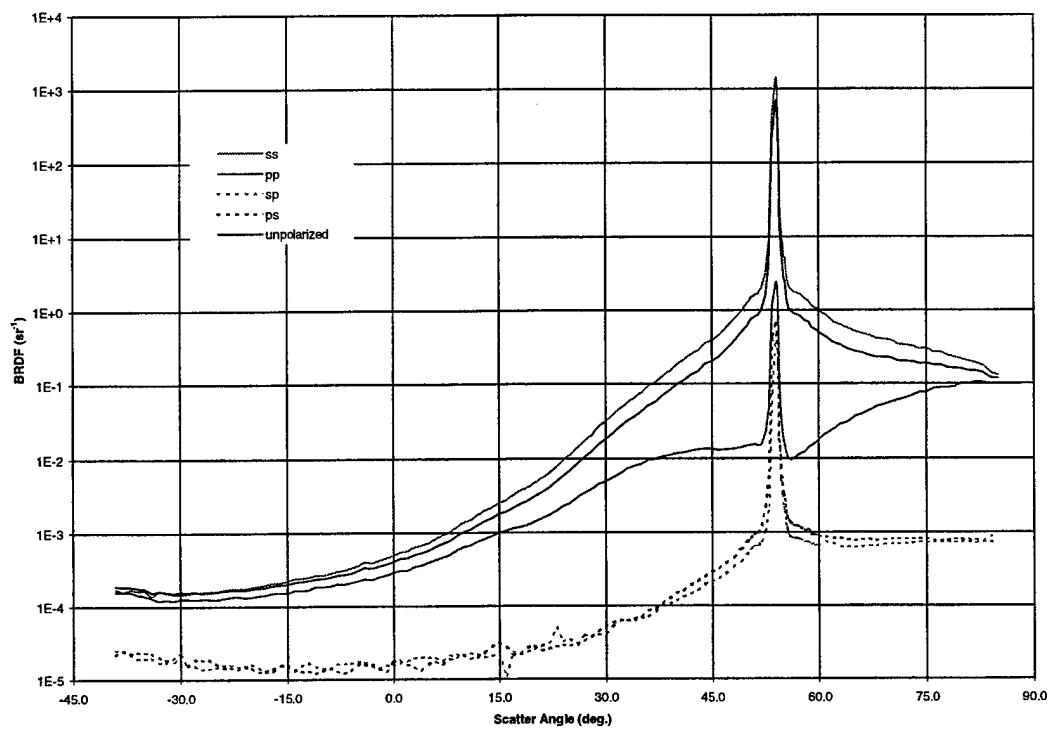
Figure 15. Polarized BRDF of sample 552_3_1.
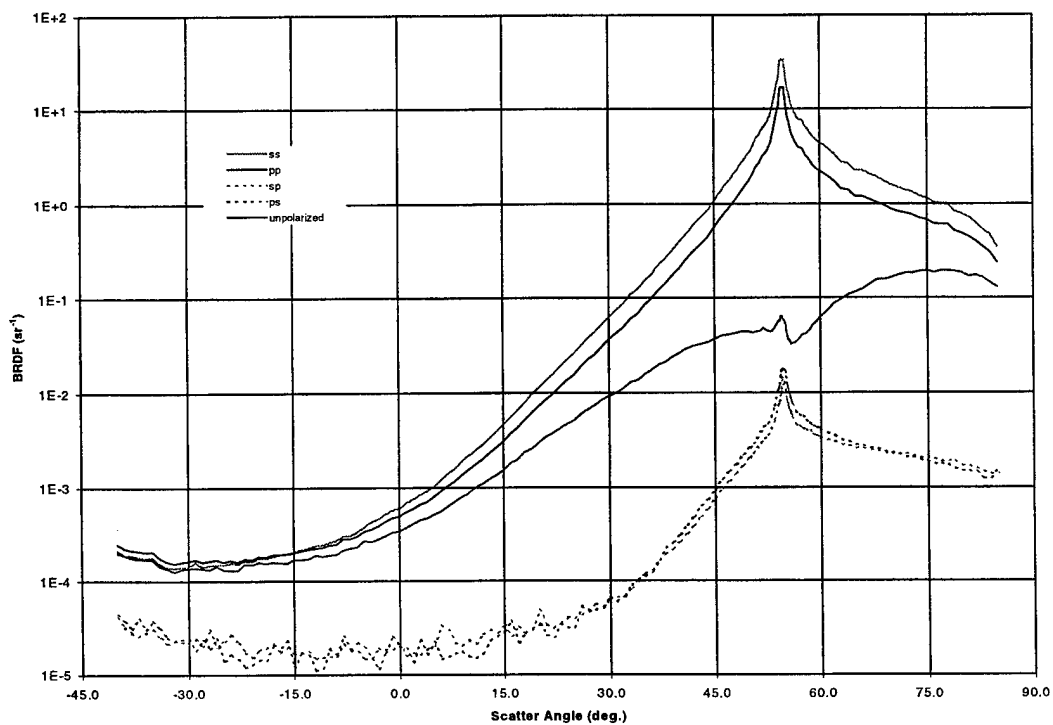
Figure 16. Polarized BRDF of Sample 552_1_1.

29
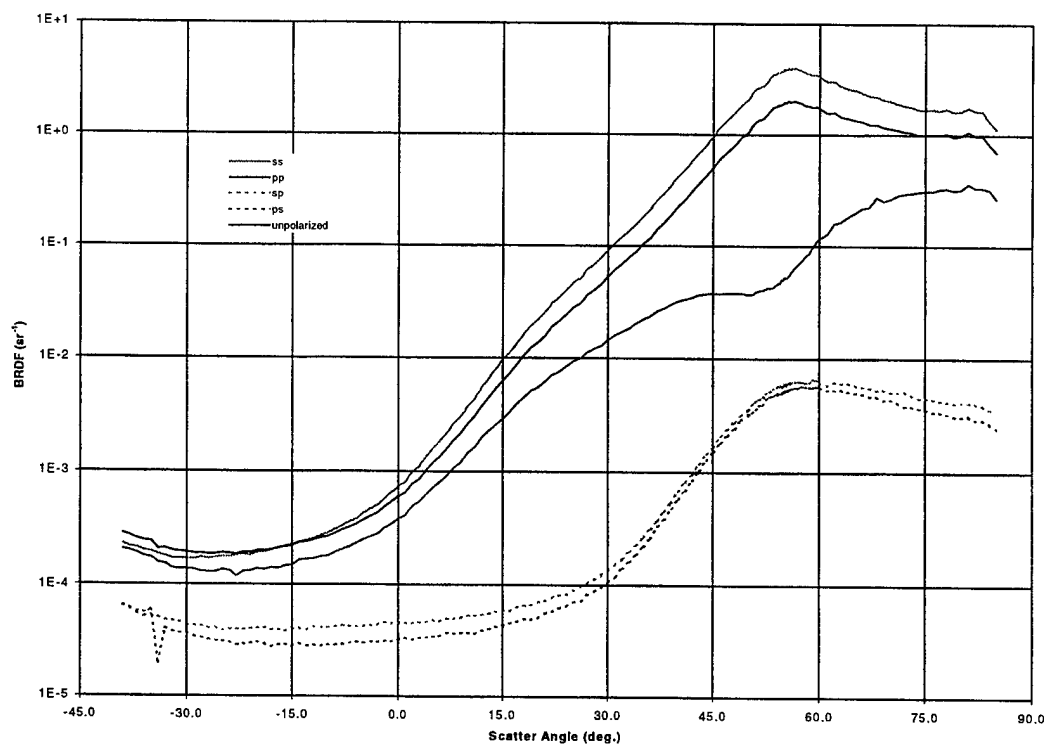
Figure 17. Polarized BRDF of sample 552_1_3.
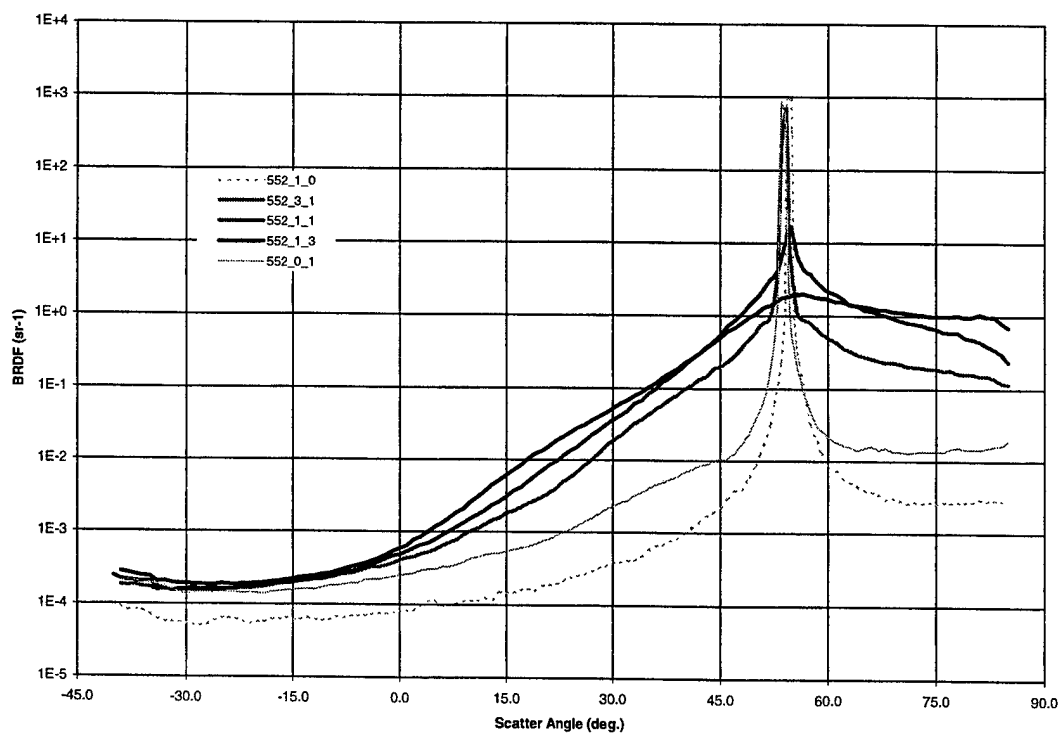
Figure 18. Unpolarized BRDF of 552 series of films.

30
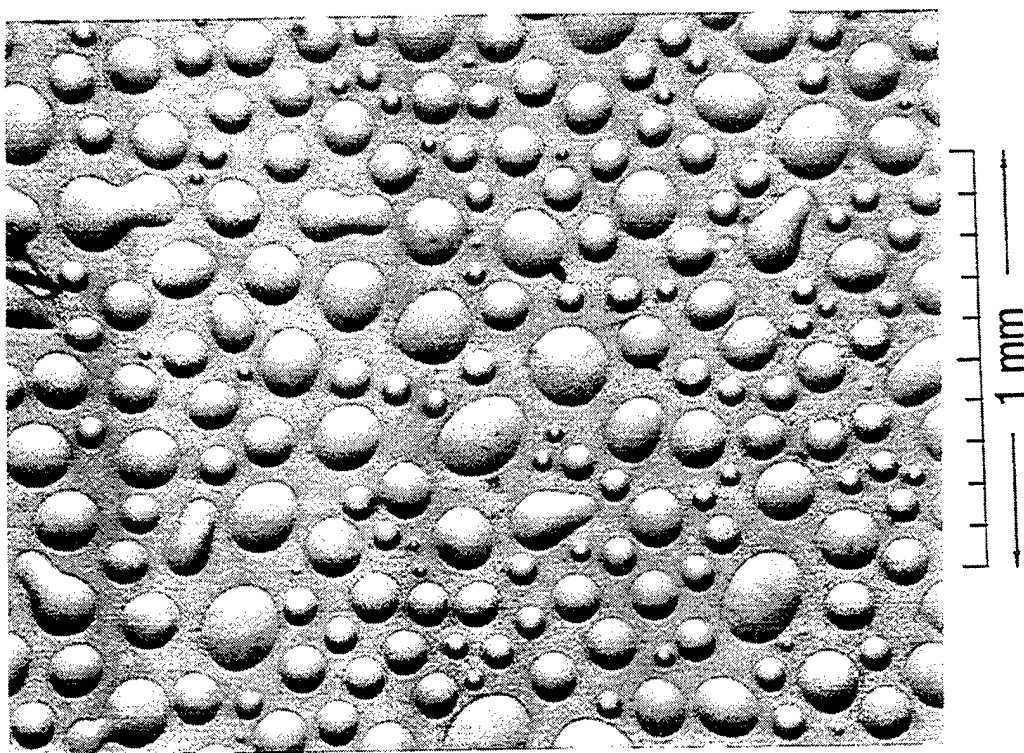
Figure 19. Light transmission photomicrograph of sample L522_1_1.
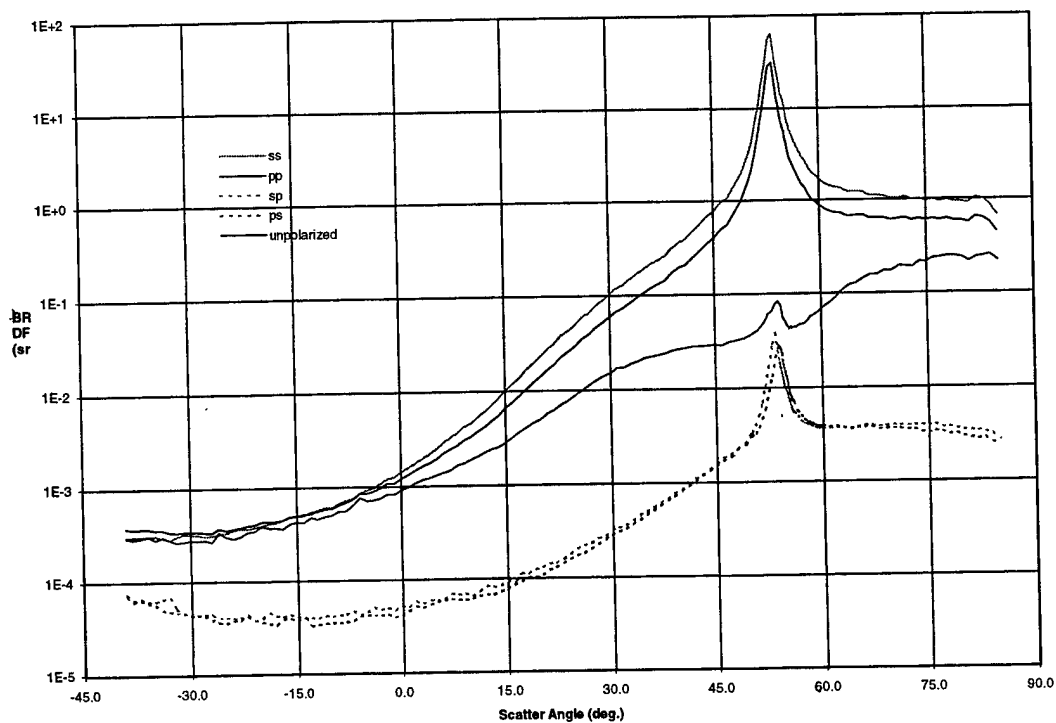
Figure 20. Polarized BRDF of sample L552_1_1.

31
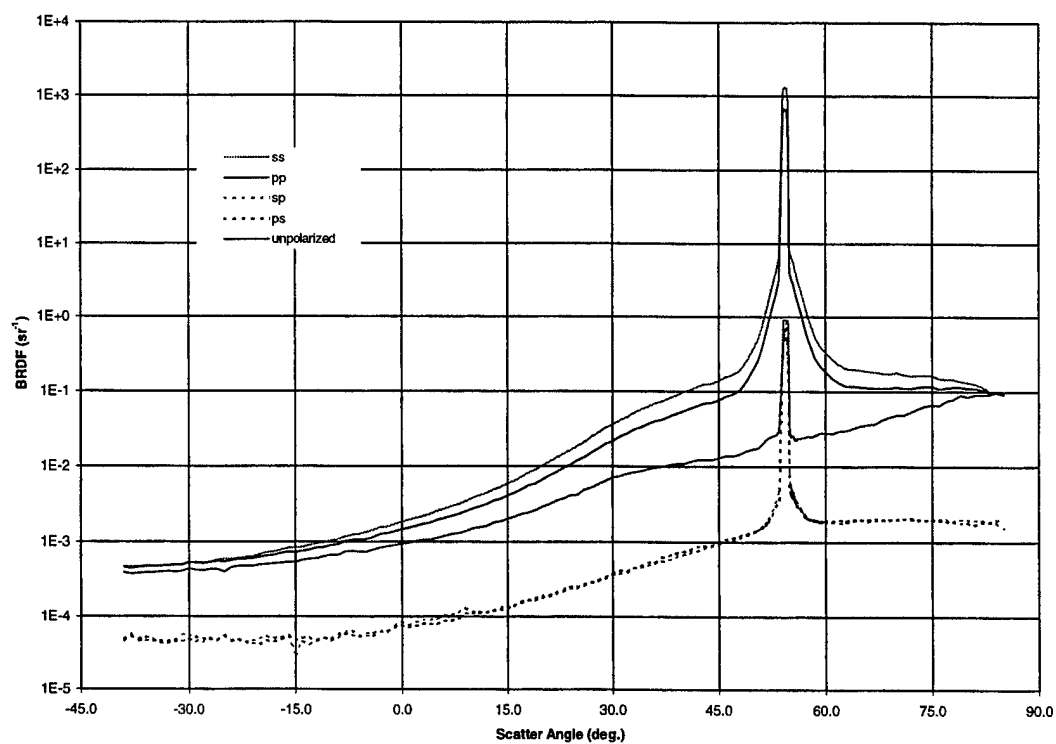
Figure 21. Polarized BRDF of sample L552_3_1.

Figure 22. Light transmission photomicrograph of sample L200_1_1.

32
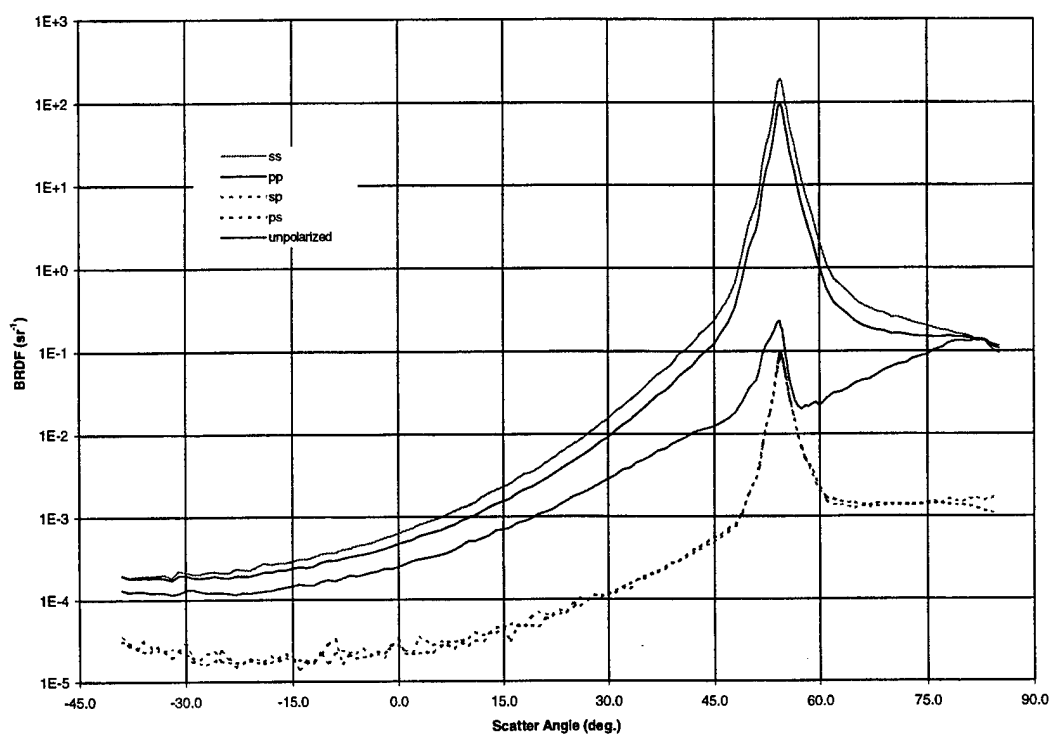
Figure 23. Polarized BRDF of sample L200_1_1.
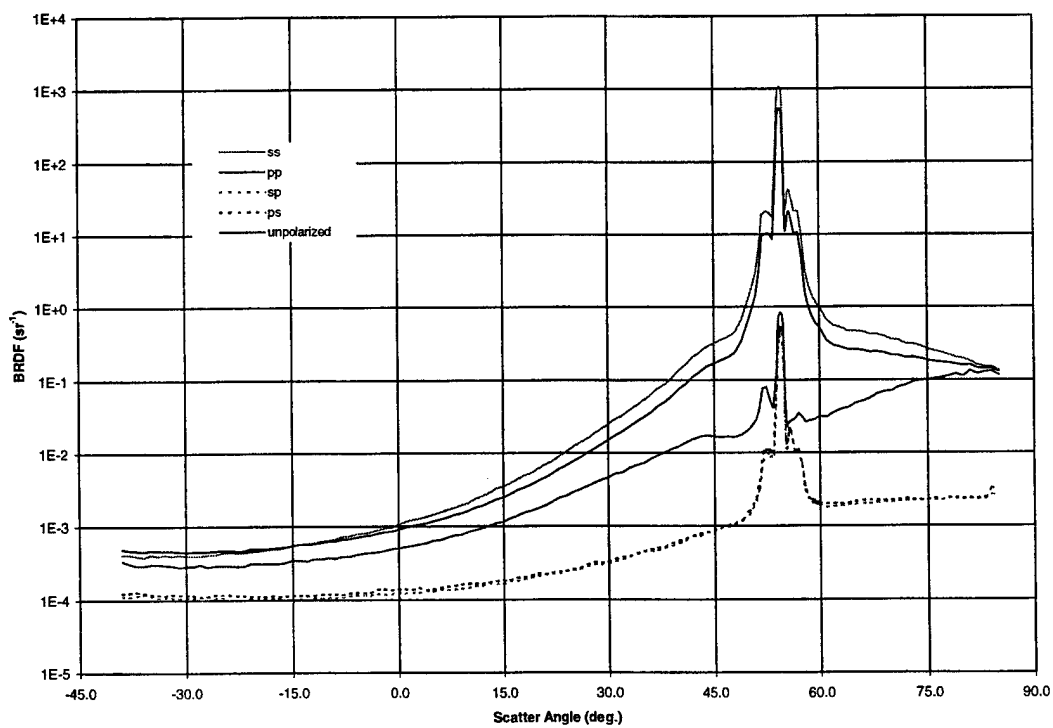
Figure 24. Polarized BRDF of sample L200_1_1.

33

40

35

30   ■ Counts on y-axis

25   ☐ Counts on x-axis

20

15

10

5

0

4   15   19   23   27   33   38   49   61   72   83   95   106 121 148

Bubble Diameter (μm)
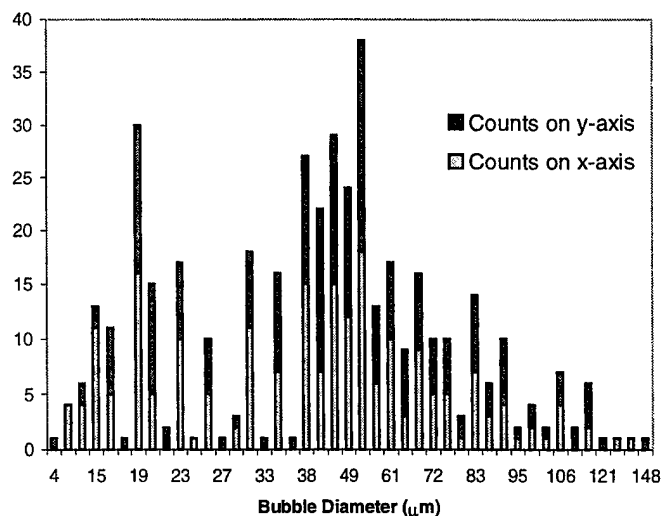
Figure 25. Approximate distribution of inclusions for sample 552_1_3.

d. Discussion and Recommendations for Further Work

The size of our experimental light scattering matrix was sufficient to show conclusively that the BRDF of unpigmented compatibilized immiscible polymer blends depends on the spatial frequency content of the morphology revealed in light transmission microphotography performed at modest magnification. The scope of these exploratory experimental and analytical efforts was too narrow to define the central structure-property relationship in enough detail to aid materials design. For example, the contributions to light scattering from the geometric surface of the film could not be separated from those from internal scattering originating with the discontinuities in refractive index at the interface of the inclusion and continuous polymer matrix. In short, we were unable to evaluate the relative importance of inclusion size and refractive index difference in diffuse scattering and gloss reduction, but the methodology is sound.

An exact description of the nature of the scattering functional relationship is a difficult modeling task that will require significant resources to pursue to a satisfactory conclusion. An empirical approach is recommended as a first step aimed at identifying and prioritizing the major extensive and intensive structural parameters governing scattering in the alloy systems. A series of samples should be produced in which the size and concentration of the volume discontinuities and their refractive index relative to the continuous matrix are systematically varied. Transmission microphotography and imaging FTIR spectroscopy should be performed to characterize the test systems. The Fourier transform of both types of images should be compared to the BRDF and analyzed for an explicit mathematical dependence.

Test samples suitable for method development can be produced in alternative ways to fully reacted polymer blends. For example, simply made blends of vegetable oil and poultry eggs (i.e. mayonnaise) could be devised that simulate the morphologies and refractive indices of practical polymer alloy systems and that exist in a stable form long enough to complete light scattering studies. The methods developed with the simplified analog systems could be transferred to selected polymer blend systems to verify the model for unpigmented films. The effect of pigment loading including gradients in the pigment concentration can then be addressed. Photomicroscopy will likely not be a useful tool for opaque samples, but its utility might be enlarged through correlation with FTIR spectroscopy.

4. Thermomechanical Properties of Clear Films Through DMA

Dynamic Mechanical Analysis (DMA) is used to characterize the mechanical response of unpigmented and pigmented polymer films. The viscoelastic properties manifested in DMA can provide a basis for a meaningful correlation of film structure with performance properties like toughness, flexibility, hardness, durability, and wear. In addition, comparison of the response of unpigmented monolithic polyester and fluoro urethanes with that of the blends might provide a gauge for the strength of interaction between the polymer phases comprising the incompatible blends. Finally, comparison of unpigmented and pigmented film response for similar resin systems will provide insight into pigment-matrix interaction mechanisms.

The clear film data presented in this Section are insufficient in scope, particularly in the time regime (frequency), to support development of a comprehensive model for the rheology of the blends. The data are sufficient to elucidate the dependence of key mechanical properties on the polyol chemical structure and on composition. The phrase 'polymer alloy' supposes that the interface between discreet phases of an incompatible polymer blend can transfer applied stress as a result of cross linking between phases (Figure 1). Otherwise, the interface is essentially an empty void supporting Van der Waals interaction that exerts an effect on the mechanical response akin to plasticization, i.e. a physical mixture. The stress transfer ability of the interface should be manifested in the storage (real) and loss (imaginary) terms comprising the (complex) modulus. In principle, a polymer alloy may exhibit equal or greater modulus than either parent. Conversely, a superposition of the signature modulus of each phase within a simple mixing rule would signify a physical mixture. The weaker inter phase interaction of a physical mixture also tends to preserve the polymer glass transition, T_g, of each polymer phase. The glasslike to rubberlike transitions may be visualized in tan δ (=loss modulus/storage modulus). Hence, modulus and/or tan δ can signal polymer alloying depending upon the how the signature properties of each phase combine to define the blend. Conditions favoring conclusive diagnosis of alloying through DMA include large differences in modulus and/or T_g for the individual polymer phases and adequate representation (mass) of each phase in the blend.

DMA was performed on films of a thickness representative of aircraft paint coatings using a method that measures the dynamic force and phase needed to maintain a prescribed extension of a test film subjected to pure oscillatory tension. The oscillation frequency and temperature are key experimental parameters that may be independently varied to map the thermomechanical response of the film. The instrument is a TA Instruments DMA 2980 Dynamic Mechanical Analyzer. All of the present data were gathered at a single oscillation frequency of 1 Hertz and over a temperature range of − 125 C to +125C. This temperature range encompasses the total of interesting structural transitions for the monolithic polyester and fluoro urethanes and the polymer alloys. Other important instrument parameter settings include static applied force (0.01 to 0.05 N), static film extension (125%), and oscillation amplitude (20 micrometer).

Clear film samples for DMA were cut from films solvent cast on glass substrates that were air cured for at least seven days and lifted from the substrate. Typical approximate sample dimensions for DMA were 12 mm (gauge length), 6 mm (width), and 0.05 mm (thickness).

The measurement results are conveniently summarized through the storage and loss terms of the (complex) modulus and their ratio, tan δ. The modulus terms are derived from the measured force components through multiplication by form factors. The form factors are constructed from measured specimen dimensions. Hence, modulus is subject to error experienced in the dimension measurements. In contrast, the location of the peak in tan δ in temperature that is commonly used to define the polymer glass transition temperature is a materials structure property sensibly independent of sample dimensions.

The uncertainty in the form factors must be managed. A caliper with a realistic uncertainty of about 0.01 mm was used to measure film width. The DMA automatically obtains gauge length to at least this resolution on the basis of a sample holder calibration of higher accuracy. Uncertainties in film width and gauge length can be arbitrarily reduced below any reasonable figure simply by taking advantage of the generous size permitted these two dimensions in the measurement cell. The sample widths and lengths employed in the present measurements reduced the uncertainty in these dimensions below 1%. The uncertainty in film thickness proved harder to manage because this dimension is dictated by the application to be the range one to three mil (~25 to ~75 micrometer). The caliper used for the length and width measurements could introduce 50%-100% uncertainty into the thickness measurement so we used instead a Sloan Technology, DEKTAK IIA profilometer having a vertical resolution of ~10^{-3} micrometer to measure film thickness. The profilometer probe was run across a step from the glass substrate on which the film was cast to the top surface of the film and along the film surface for some millimeters to appraise flatness and surface roughness. Accumulated profilometer scans revealed that the variation in thickness over the sample gauge length replaced thickness measurement accuracy as the central factor determining form factor uncertainty. In summary, management of dimensional uncertainty brought film-to-film consistency to an acceptable level in the DMA measurements. However, uncertainty in the derived quantities remained sufficiently high due to variations in the film thickness

over the gauge length to necessitate evaluation of experimental precision through repeat DMA measurements on nominally identical films.

The storage modulus and tan δ from oscillating pure tension force measurements on clear film samples of 100% fluoropolymer urethane, 100% polyester urethane, and 75:25, 50:50, and 25:75 blends are given in Figures 26, 27, and 28, respectively. Checks on experimental precision are reported in Figures 29 and 30. The series of clear film samples include the compositions described in Table 1, but the NCO:OH index is maintained constant at 1.60 in the DMA films to preclude variable urea/urethane linkages. The thickness of the films lay in the range 0.025 to 0.050 mm (1-2 mil). According to Figures 29 and 30, the apparent reproducibility of the DMA measurement of storage modulus is 14%. The major contributor to the imprecision likely is unresolved variation in film thickness over sample gauge length. The glasslike to rubberlike transition temperature indicated by the tan δ peak is reproduced within 3 degrees Celsius.

Comparison of storage modulus and tan delta
of monolithic fluoro and polyester urethanes
[DMA of clear films, NCO:OH index=1.60]
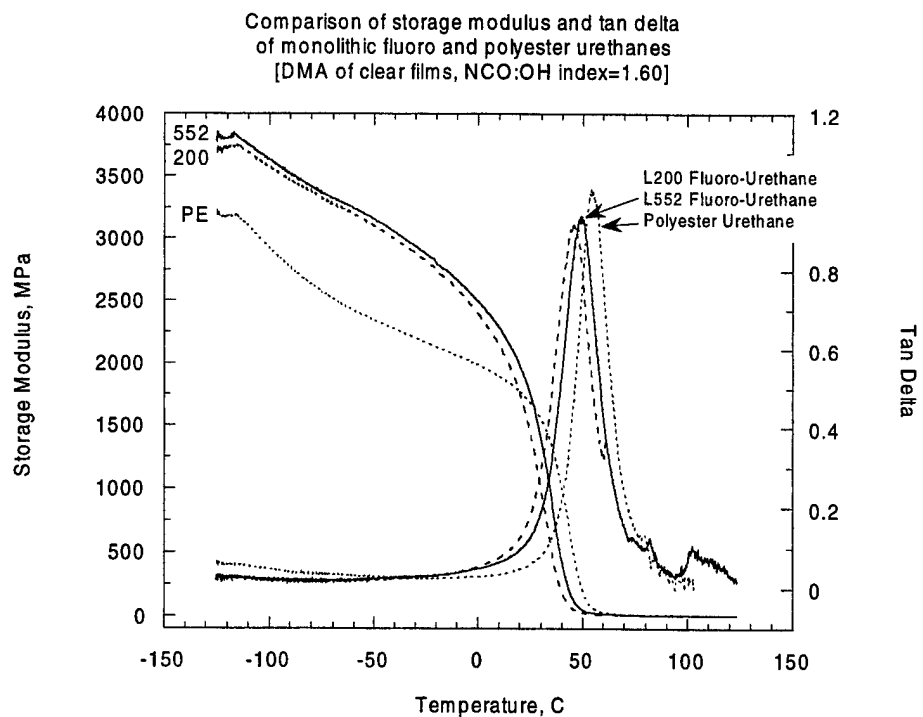
Figure 26. Storage modulus and ratio of loss modulus to storage modulus for the monolithic urethanes used to create the polymer alloys in the present work.

Storage modulus and tan delta for L200:polyester alloy series
DMA of clear films, NCO:OH=1.60
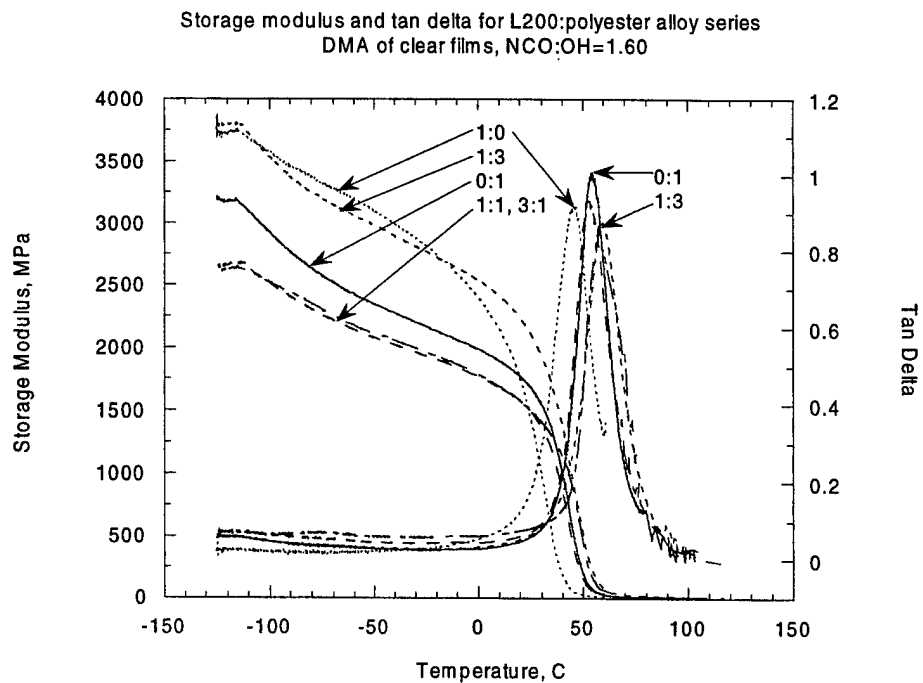
Figure 27. Storage modulus and tan delta for the polymer alloy series based on the fluoro polyol L200 and polyester polyol compatibilized with isocyanate.

38

Storage modulus and tan delta for L552:polyester alloy series
DMA of clear films, NCO:OH=1.60
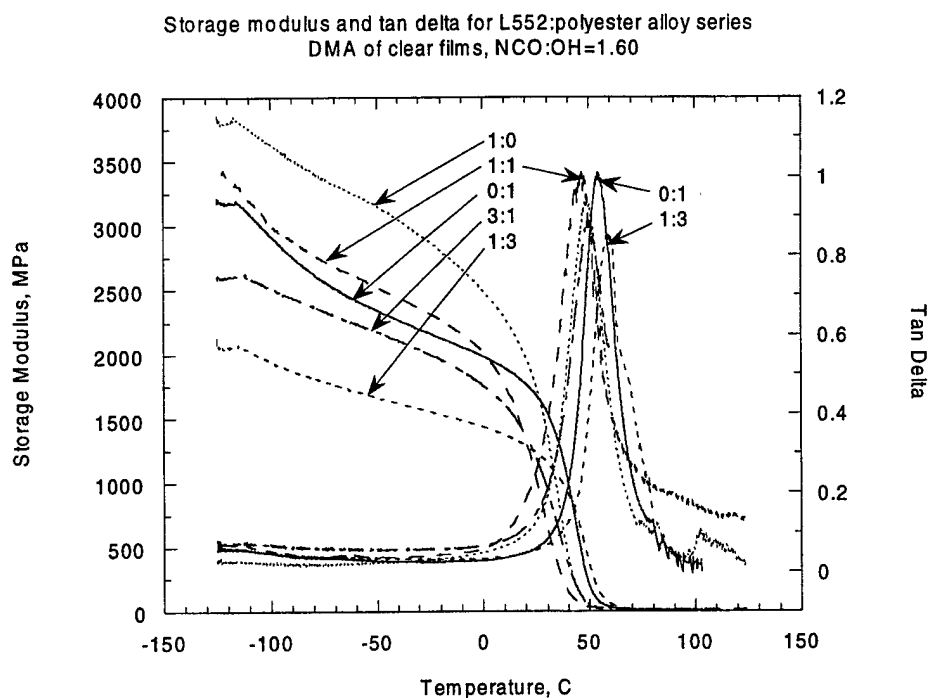
Figure 28. Storage modulus and tan delta for the polymer alloy series based on the fluoro polyol L552 and polyester polyol compatibilized with isocyanate.

Storage modulus and tan delta for monolithic polyester urethane
[comparison of two DMA measurements on two film samples
from same cast clear film]
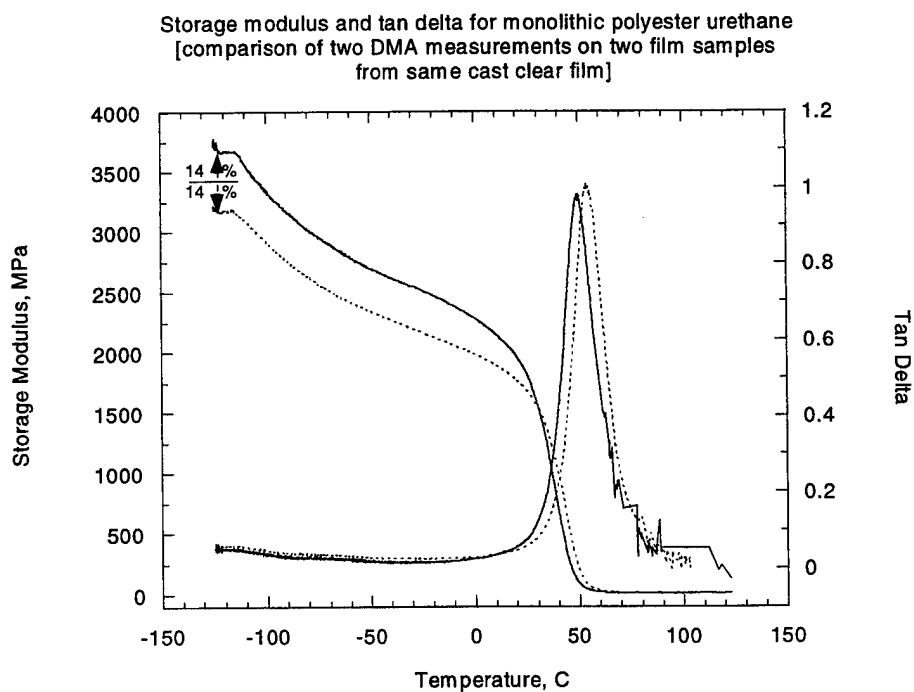
Figure 29. Comparison of two DMA measurements on nominally identical clear films of the polyester urethane to indicate experiemental precision.
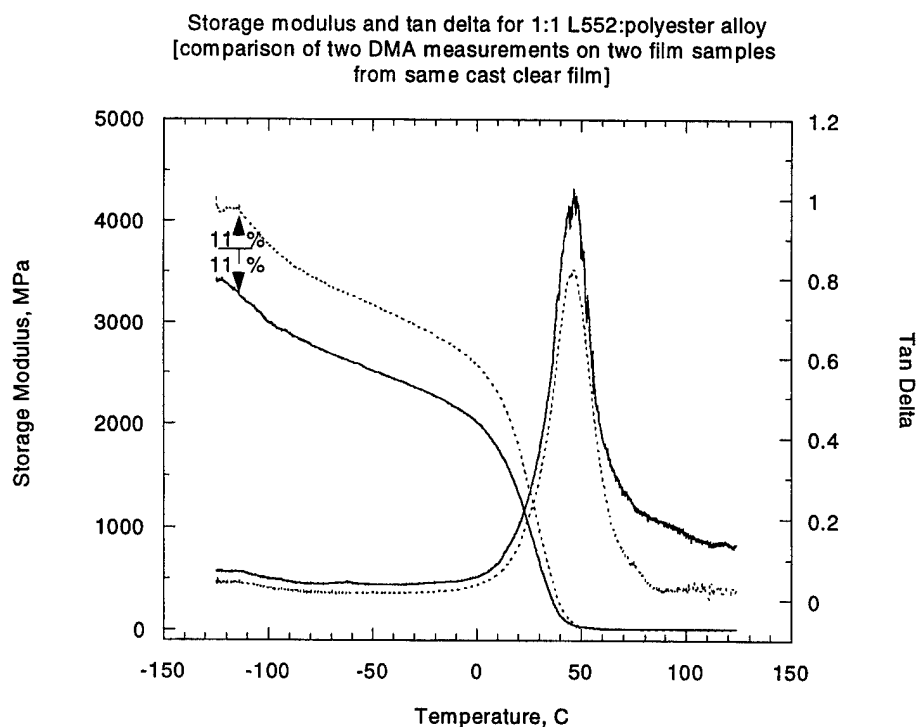
Figure 30. Comparison of two DMA measurements on nominally identical clear films of a fluoro polyester urethane alloy indicating experiemental precision.

We proposed that a clear signal for polymer alloying would be the storage modulus for the blends equaling or surpassing the lowest parent urethane and/or the blend tan δ showing a single peak representative of the alloy rather than two for the physical blend. The baseline behavior for gauging either of these occurrences is in Figure 26. These data show the fluoro urethanes have equal storage modulus and T_g. The fluoro urethane modulus apparently exceeds the polyester urethane modulus and its T_g lies about 9 C below that of the polyester urethane. The difference in the magnitude of the storage modulus for the fluoro and polyester urethanes in Figure 26 cannot be considered significant in view of the 14% experimental precision for this quantity. The difference of 9 C in T_g is significant in view of the 3 C experimental precision.

The series of blends (Figures 27 and 28) exhibit a storage modulus in the range 2200-3800 MPa at low temperature and a glasslike to rubberlike transition in the range 45 C to 59 C. The modulus of a blend exceeds one parent only for the 1:3 composition in the L200:polyester system (Figures 27), and only for the 1:1 blend in the L552:polyester system (Figure 28). The 1:3 blend in the L552 series exhibits the lowest modulus of all tested and is the only one to fail to equal a parent urethane within the 14% precision of the modulus measurement. No superposition of the parent modulus or tan δ is evident in either series of blends. We note however that the modulus and T_g for the polyester and fluoro urethanes are sufficiently alike to make recognition of a simple weighted superposition difficult within the experimental uncertainty.

40

Consider now if film morphology might correlate with the variation in blend modulus. A central feature of one type of blend morphology (Section 4 c 2 and 4 c 3) is a spherical (or perhaps oblate spheroid) included phase several 10's of micrometers in diameter within a continuous matrix. The included phase is primarily polyester urethane through 1:1 that inverts to primarily fluoro urethane by 1:3. The 1:1 L200 and L552 blends are both in this group but their modulus and T_g differ. The 1:3 L552 blend is also in this group but its modulus is considerably below 1:1. Indeed, the modulus for 1:3 L552 might be considered low enough to signal plasticization except that the otherwise similar 1:3 L200 blend gives large irregular polyester urethane particles, high modulus, and the highest T_g in the L200 series.

The 3:1 L200 and L552 compositions form a separate morphological group. The central feature of this group is polyester urethane inclusions within a fluoro urethane matrix of a size below the resolution limit of the IR microscope. The presence of the unresolved inclusions can be inferred from the opaqueness of the films. Further, their BRDF manifest a strong specular scattering component that attests to a narrowed size distribution (Section 4 c 3). The modulus for 3:1 for both fluoro polyols tends to fall at the low end of their respective composition ladders.

It is evident from this discussion that the modulus and tan δ reveal no obvious systematic variation with morphology as composition and inclusion size and shape vary over wide ranges.

We conclude that our rheology data are too limited in scope to define general boundary conditions for polymer alloy formation from systematic alterations in the modulus or glass transition. But taken on their own merit the modulus and tan δ results in Figures 26-28 show definitively that the fluoro polyester resin system provides a basis for a low gloss coating system that need make no sacrifice in the mechanical or thermal properties attainable with the individual parent resins. If we invoke here the screening test results for the fully pigmented 1:1 blend topcoat systems presented subsequently, we can associate the modulus and tan δ for at least the 1:1 system with enhanced toughness and wear that meet full expectations for a polymer alloy. We conclude that the relative magnitude of the DMA modulus and the single peak in tan δ for the blends are consistent with polymer alloy formation for all compositions except perhaps the 1:3 L552:polyester blend. A more comprehensive model for blend rheology is needed for appraising inter phase cross link density and the influence of phase morphology on thermomechanical properties. This task requires more extensive and higher resolution DMA especially in time domain (frequency) than was achieved in the present work.

5. Thermomechanical Properties of Pigmented Films Through DMA

The two polymer alloy matrix systems featured in Figures 26-30 were fully pigmented to a hiding power and Federal standard color typical of modern high quality aircraft topcoats, and their thermomechanical response was measured in DMA following procedures previously described. Pigmented films were cast from solvent on a glass

substrate and air dried for at least 7 days. The dry film was scored and a portion lifted from the substrate by immersing the film slowly into water. DMA samples approximately 12 mm (length) x 6 mm (width) x 0.05 mm (thickness) were cut from the free standing film, dried, and mounted in the DMA thin film tension clamp.

The DMA storage modulus and tan δ for the two pigmented systems are compared to the unpigmented resin systems in Figures 31 and 32 to illustrate pigment reinforcement. Consequences of a strong pigment polymer interaction are evident in the large increases in storage modulus and polymer glass transition temperatures. Pigmentation diminishes the lossiness, or tan δ, of the polymer alloy matrix. The two fluoro polyols show similar degrees of change in storage modulus and tan δ with pigmentation.

Pigment reinforcement of L200 fluoro polyester urethane alloy
through DMA modulus
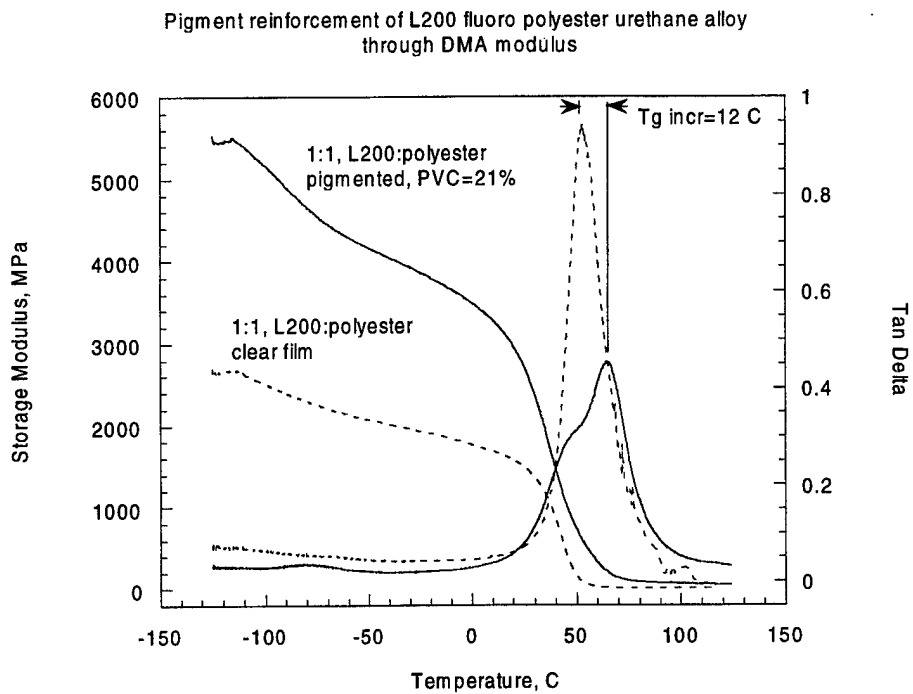
Figure 31. Pigment reinforcement of 1:1 L200:polyester alloy resin system. The fully pigmented topcoat designation is FP_PU_3F.

Pigment reinforcement of L552 fluoro polyester urethane alloy
through DMA modulus
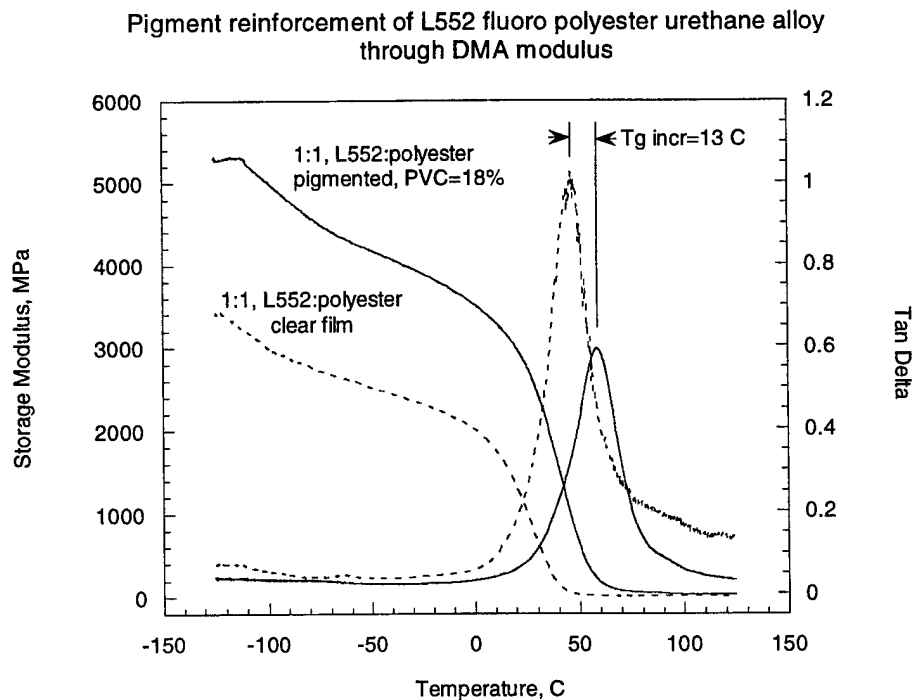
Figure 32. Pigment reinforcement of 1:1 L552:polyester alloy resin system. The fully pigmented topcoat designation is FP_PU_22.

43

Both terms of the modulus must be considered together to understand certain features appearing in tan δ in Figures 31 and 32 and to begin to connect the film parameters probed in DMA to macro properties of the paint films that are measured in standard screening tests. The real (storage) and imaginary (loss) modulus terms for the pigmented and unpigmented films of the two fluoro polyester urethane systems are given in Figures 33 and 34. We restrict our attention to the strong α relaxation above 20 C. The temperature dependence of the loss term differs for the L200 and L552 fluoro polyester urethanes. Pigmentation shifts the maximum in the loss modulus 14 C higher in the L552 system and 2 C or less in the L200 system. The small pigment induced shift in the L200 system is responsible for the bimodal structure in tan δ near T_g (Figure 31). Physically, the shape of tan δ may signify preferential concentration of pigment in one phase of the phase separated system, but this supposition could not be independently verified. The scope of our DMA experiments is too limited particularly in the time domain to support a detailed model interpretation.

The DMA measurements enable an association of the macro property of film elongation with a more fundamental continuum measure of embrittlement. Film elasticity or elongation is characterized by GE Impact at failure in screening tests. GE Impact for the unpigmented polymer alloy systems was measured to be greater than 60%, this figure representing the upper limit for the measurement for any film on a 2024 T0 aluminum substrate. It will be shown subsequently that pigmentation lowers GE Impact to the range of 20-40%. The drop in GE Impact may be associated with changes in the more fundamental quantities of DMA storage modulus and tan δ (Figures 31, 32), and loss modulus (Figures 33, 34). Specifically, the data show that a drop in GE Impact to 20-40% corresponds to a 60% increase in DMA storage modulus below T_g and, though tan δ decreases, a simultaneous 40% increase in loss modulus.

Pigment reinforcement of L200 fluoro polyester urethane alloy
through DMA modulus
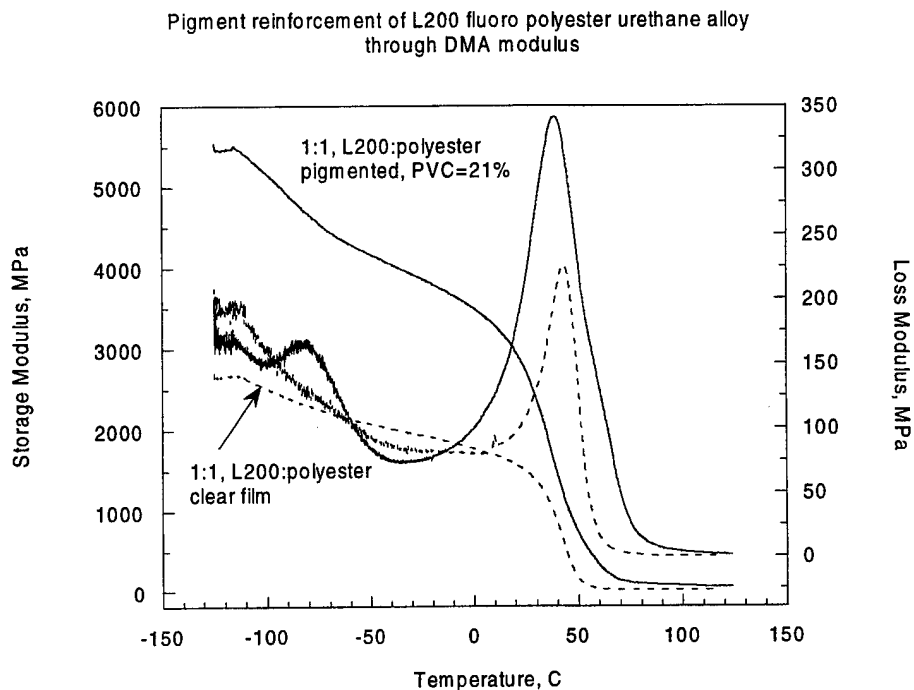
Figure 33. Real and imaginary terms of the modulus for the 1:1 L200:polyester alloy resin system, topcoat designation FP_PU_3F.

Pigment reinforcement of L552 fluoro polyester urethane alloy
through DMA modulus
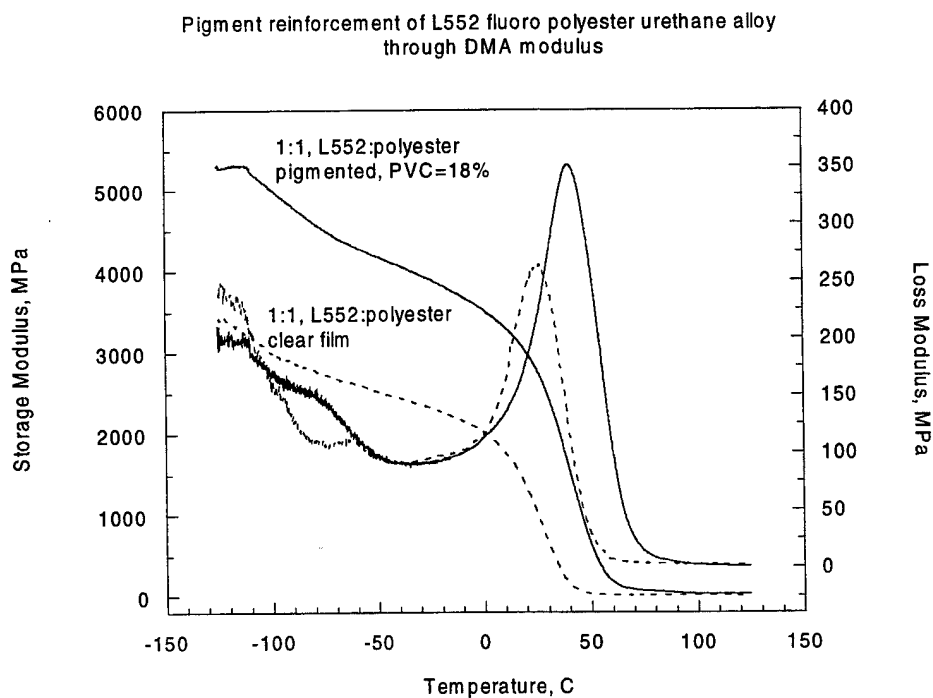
Figure 34. Real and imaginary terms of the modulus for the 1:1 L552:polyester alloy resin system, topcoat designation FP_PU_22.

6. Screen Testing of Pigmented Systems

Fully pigmented polymer alloy resin systems were created to evaluate the feasibility of polymer alloys for ultra low gloss topcoat systems. Screen test samples were sprayed onto 3 inch x 6 inch or larger aluminum sheet panels. The substrates destined for gauging film elasticity through GE Impact at Failure were unprimed 2024 T0 aluminum. The substrates for all other tests were primed 2024 T3 aluminum. Sprayed coatings were air dried 14 days or subjected to an accelerated cure consisting of 24 hours at air ambient followed by 48 hours in a 125 ^{0}F oven.

Results[4] from screening tests commonly used to relate certain optical and mechanical properties to the composition and processing of the paint film are given in Table 5. The resin systems are 50:50 and 75:25 blends of the L552 and L200 fluoro polyols with a polyester polyol compatibilized with an aliphatic polyisocyanate. The systems are sufficiently near color/gloss targets to permit comparison of properties without fear that further color adjustment might alter test rankings. The objective of the formulation ladders presented in Table 5 is to provide general insight into the influence of important formulation parameters (PVC, NCO:OH index) on a few selected properties deemed significant to predicting coating performance. Comments on the stability of the color pigment suspension are offered in Table 5 to indicate the sensitivity of pigment stability to the polyol structure.

Table 5. Pigmented Polymer Alloy Systems Test Results

Sample	PVC (%)	Syloid[1]	NCO:OH	$60^0/85^0$ gloss	GE Impact[2]	PH[3]	color pig.
50:50 L200:670[4]	20.7	29.8	1.60	4.0/4.0→ 8.0/8.7	40 @ 2.0	pass2H-4H fail 4H-6H	stable suspension
75:25 L200:670[5]	19.9	22.8	1.60	5.2/6.6	10 @ 2.0	pass2H-4H fail 4H-6H	color pig. float
50:50 L552:670[6]	18.4	16.4	1.60	3.9/4.2	40 @ 1.8	pass 2H-4H fail 4H-6H	color pig. float
75:25 L552:670[7]	18.8	16.4	1.60	12.3/17.3	40 @ 2.0	pass2H-4H fail 4H-6H	color pig. float
50:50 L552:670[8]	18.3	16.4	2.30	1.9/3.3	10 @ 1.8	pass2H-4H fail 4H-6H	color pig. float

1. Syloid 620 concentration as weight percent of solid pigments (color plus extender).
2. GE Impact at Failure at DFT (dry film thickness in mil). Values given represent average behavior based on results for three or more films.
3. Pencil hardness. Values represent the expected behavior based upon results for three or more films.
4. BBM designation, FP_PU_31 and _3F. The latter is the final system sent to Battelle. The stated gloss values indicate the range experienced with variations in processing and are discussed in the text. The GE Impact for this system represents a crude average of a maximum value of 60% obtained for one or two test films, 40% for some films, and a minimum of 20% for others.
5. BBM designation, FP_PU_40.
6. BBM designation, FP_PU_22.
7. BBM designation, FP_PU_25.
8. BBM designation, FP_PU_23.

The clear film pencil hardness data (Table 1) and morphology analysis (Section 4 c 2 and 4 c 3) considered with analogous data for the pigmented films in Table 5 support the supposition that the fluoropolymer forms the continuous phase in the pigmented 50:50 and 75:25 fluoro:polyester films. It can be stated even at this early stage of evaluation that both fluoro polyols show good promise as the basis with polyester polyol for a pigmented polymer alloy system that is low gloss and hard and yet reasonably elastic.

The dependence of gloss on PVC measured in a separate ladder study[4] of the L200 and L552 fluoro polyol systems of Table 5 is shown in Figure 35. A representation[2] of the average behavior of the pigmented 50:50 L552:polyester alloy is included in Figure 35 for completeness. The variation in PVC over the range depicted was accomplished through adjustment in the Syloid 620 extender pigment loading.
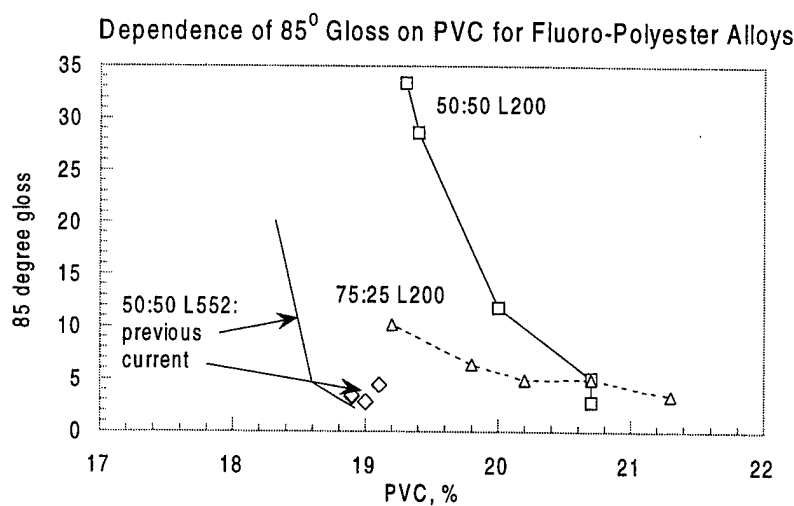
Figure 35. Dependence of 85 degree gloss on PVC for three fluoro polyester urethane alloy systems.

Environmental stability of the pigmented polymer alloy systems was evaluated through standard oil and water immersion tests. The results[4] are summarized in Table 6. Gloss, PH, and GE Impact were followed as far as possible for a specific sample panel to better gauge the change wrought by fluid exposure.

Table 6. Pigmented Polymer Alloy Behavior in Fluid Immersion Tests
(Oil, 24 hour immersion at 250 ^{0}F. Water, 4 day immersion at 125 ^{0}F.)

Sample	PVC (%)	NCO:OH	$\Delta 60^0/85^0$ gloss	color $\Delta\Delta E^3$		GE Impact[1]	PH[2]
H$_2$O; 50:50 L200:670[4]	20.7	1.60	Δ= 0.8/0.6	0.3	initial value- final value-	40 @ 2.0 20 @ 1.9	pass 3H pass F, 2H
Oil; 50:50 L200:670[4]	20.7	1.60	not measurable	0.2	initial value- final value-	40 @ 2.0 40 @ 1.6	pass 3H pass H
H$_2$O; 75:25 L200:670[5]	19.9	1.60	Δ= <1/<1	0.2	initial value- final value-	10 @ 2.0 20 @ 1.7	pass 2H pass H
Oil; 75:25 L200:670[5]	19.9	1.60	not measurable	0.4	initial value- final value-	10 @ 2.0 40 @1.6	pass 3H pass 2H
H$_2$O; 50:50 L552:670[6]	18.4	1.60	Δ= <1/<1	0.3	initial value- final value-	40 @ 1.8 40 @ 1.1	pass 2H pass F, H
Oil; 50:50 L552:670[6]	18.4	1.60	not measurable	0.5	initial value- final value-	40 @ 1.8 40 @ 1.6	pass 3H pass 2H
H$_2$O; 75:25 L552:670[7]	18.8	1.60	not measured	0.1	initial value- final value-	40 @ 2.0 20 @ 1.3	pass 3H pass F, H
Oil; 75:25 L552:670[7]	18.8	1.60	not measurable	0.3	initial value- final value-	40 @ 2.0 40 @ 1.6	pass 3H pass 2H
H$_2$O; 50:50 L552:670[8]	18.3	2.30	Δ= <1/<1	0.2	initial value- final value-	10 @ 1.8 not measrd	pass 2H pass H
Oil; 50:50 L552:670[8]	18.3	2.30	not measurable	0.3	initial value- final value-	10 @ 1.8 not measrd	pass 2H pass H

1. GE Impact at Failure at DFT (dry film thickness). Post test value acquired within five minutes after removal from fluid.
2. Pencil hardness. The post test value acquired within five minutes after removal from fluid. In two water tests, PH was followed for two hours to measure hardness recovery following removal from the water. Where two values of final PH are given, the first represents the PH immediately after removal and the second the PH recovered after 45 minutes to 2 hours at air ambient. A single given value generally corresponds to the recovered value. Recovery was not examined for oil.
3. Change in the deviation in color E value from standard. The post test value was acquired within five minutes after removal from fluid.
4. BBM designation, FP_PU_31 and _3F. The latter is the final system sent to Battelle.
5. BBM designation, FP_PU_40.
6. BBM designation, FP_PU_22.
7. BBM designation, FP_PU_25.
8. BBM designation, FP_PU_23.

The data of Figure 35 and Tables 5 and 6 suggest:

1. All systems are color stable in that all show negligible change in color through the water and oil tests (Table 6). What is *not* evident in either Table 5 or 6 is the large difference from target color standard for some of the systems. The stability of color

pigments is discussed subsequently. Here it is sufficient to note that the 50:50 L200:polyester was the most responsive of the group to color adjustment using the surfactant and pigment packages included in the experimental matrix.

2. All of the test systems are low gloss (Table 5). That said, Figure 35 shows that the efficiency of gloss reduction depends upon the fluoro polyol and its concentration. The morphology generated with L552 evidently is the most efficient yielding the minimum PVC system studied (PVC≈18%). The 75:25 L200:polyester system is comparable in efficiency of gloss reduction while the 50:50 L200:polyester system is least efficient by about 3 PVC %. Present data are insufficient in scope to appraise the importance of the 3% difference in PVC to morphology and performance.

3. Raising the fluoro polyol content from 50:50 to 75:25 lowers elongation in the L200 system but not in the L552 system (Table 5). Water and oil plastisize 50:50 less obviously than 75:25 for L200, and not at all (or equally well) for L552 (Table 6).

4. Raising the NCO:OH reaction index degrades elongation (Table 5).

5. Four days in 125 ^{0}F DI water lowers pencil hardness two to three units, but one to two of these lost PH units are recoverable within ¾ -2 hour in air ambient (Table 6).

6. Oil exposure consistently degrades PH by one unit (Table 6). Recovery, if any, was not examined.

The 50:50 L200:polyester system exhibited the best color pigment suspension stability among the systems tested, in that color could be methodically adjusted through a calculated change in relative color pigment concentrations and quickly verified by experiment. Verification of the calculated color change was rapid because color stabilized during milling as witnessed by fairly uniform rub-ups. In contrast, the gloss of this system required some hours of standing upon milling to stabilize to a constant value. The observed drift in gloss was tolerable because gloss values remained within acceptable bounds and the final level was controllable through adjustment of the extender concentration.

The three systems other than the 50:50 L200:polyester of Table 5 required time intervals of many hours to stabilize color and, in some cases, gloss. Drift was appraised through observation of the change in color and gloss with time in a series of panels sprayed from a single reserve of 50:50 L552:polyester. Measurement results over a ten day period are given in Figure 36. Color in this system evidently requires more than 75 hours of standing to approach a constant value while gloss stabilizes quickly. We presume that the existence of an induction period in color stabilization is a manifestation of retarded wetting of the pigments by one of the two polyols. Note that pigment wetting by system polyols can always be accelerated through the use of new surfactants and/or pigment packages.
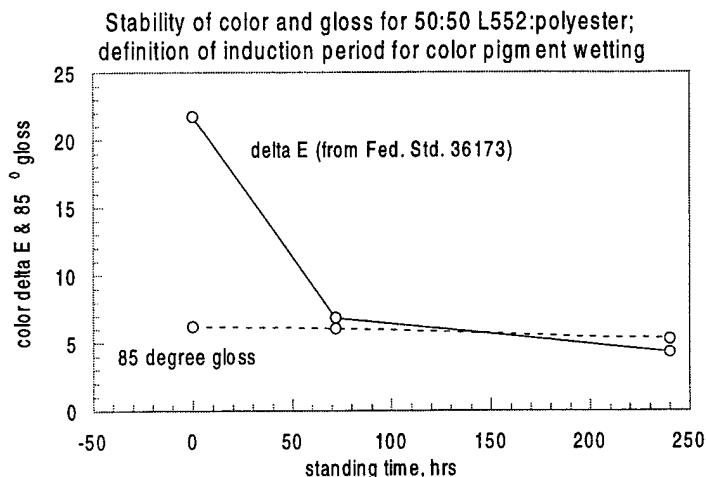
Figure 36. Induction period for color and gloss for 50:50 L552:polyester alloy system.

The 50:50 L200:polyester polyol system was selected to represent the polymer alloy concept for high performance ultra low gloss topcoat systems in an extensive evaluation by Battelle[24] of a number of candidates in an advanced performance coating program conducted by the Air Force. Our selection of this system was based on good screening test results and the fact that the requisite color standard was precisely matched. Nevertheless, the 50:50 and 75:25 L552:polyester systems remain attractive in offering a smoother surface finish as well as promise for higher average elongation than the L200 polyol with due attention paid to color matching. Selected results from the Battelle tests are presented subsequently.

7. Expanded Property Tests on Pigmented Systems

The pigmented polymer alloy system designated FP_PU_3F in Tables 5 and 6 was selected for further testing at Battelle, Columbus Laboratories, within a testing program aimed at identifying compositional factors that promote superior topcoat cleanability and durability[24]. The goals of the Battelle tests were ambitious in seeking to correlate accelerated laboratory testing with performance in the field. For this reason, the Battelle tests are broader in scope than, say typical screening tests that are performed in the course of development of a new paint system. Added value in the Battelle tests derives from comparison of three topcoat systems that differ substantively in their chemical and physical structures. Selected of these comparative data are used here to illustrate property enhancements attributable to alloying.

The three topcoat systems of interest from the Battelle study include Deft Control, Deft ELT, and TJF Solutions (FP_PU_3F). For present purposes, the Deft Control can be described as a traditional polyester urethane topcoat system made low gloss through an elevated extender pigment loading (net filler loading estimated at 47 volume %). Deft ELT is a monolithic fluoropolymer urethane that achieves low gloss with a somewhat lower pigment loading (net filler loading estimated at 35 volume %). The TJF Solutions

51

system is a fluoro polyester urethane alloy from TJF Technical Solutions, Inc. that achieves low gloss at a PVC of 21% (12% primes, 9% extender). Results of standard screening tests for the TJF polymer alloy system are given in Table 7 and the formulation is given in Table 8. Formulation details are unavailable for the two Deft systems so the cited PVC are approximate values deduced from independent TGA (thermogravimetric analysis) measurements[24]. The cited PVC for TJF Solutions system is exact.

TABLE 7. SCREENING TEST RESULTS FOR FP_PU_3F

Color in terms of ΔE from 36173 standard (goal= <2):	ΔE=0.3
85^0 gloss(goal= <3:	4.0→8.0[1]
60^0 gloss (goal= <3):	4.0→8.7[1]
DFT (goal= 2.0 mil):	3.0 mil
#4 Ford cup, initial/4 hours (goal= <35sec at 4 hours):	25.3 sec/29.5 sec
Dry time STT (goal= <3 hours):	2 hr (70^0F)
8 hour tape time (goal= <8hours):	pass
11 minute wet edge, 85^0 gloss over area 1, 2, and overlap:	sample 1: 12.5, 8.4, 10.3[2] sample 2: 7.7, 4.4, 3.4[2]
GE Impact, TO unprimed (goal= 20-40):	20 @ 2.9 mil
Low temp flex (goal= 1 inch mandrel):	not performed

Mil L 23699, 24 hr immersion at 250 ^{0}F (goals):

Color in terms of ΔE from 36173 standard	ΔE= not measured
Difference from air dried film:	ΔE=0.3
tape adhesion	not performed
60^0/$\Delta85^0$ gloss (goal= <3.0):	not measurable
GE Impact (goal= 20-40):	40 @ 3.0 mil[3]
Low temp flex (goal= 1 inch mandrel):	not performed
Pencil hardness, initial/final (goal= <1 change):	3H/H

Water resistance, 4 days at 120 ^{0}F:

Color in terms of ΔE from 36173 standard:	ΔE=0.4
Difference from air dried film:	ΔE=0.3
tape adhesion	not performed
$\Delta60^0$/85^0 gloss (goal= <1.0):	0.8/0.6
GE Impact (goal= no change):	40 @ 3.1 mil
Low temp flex (goal= 1 inch mandrel):	not performed
Pencil hardness, initial/final (goal= 0 change):	3H (initial)/F (wet) F (wet)→2H (dry)[4]

1. The range in gloss observed for at least three incarnations of FP_PU_3F is given. See discussion of pigment stability in the text for a rational.
2. A variation in the gloss is not discernible to the eye between the first sprayed area and the second area sprayed 11 minutes later nor with the overlap area, for either panel.
3. The 40% GE Impact deformation that was a pass for the oil test was observed to alter with time. Within 8 days in air ambient the 40% deformation test area developed failure cracks thereby lowering GE pass to 20%.
4. The change from 'wet' to 'dry' values of PH occurred over a ¾ to 2 hour stand in air ambient. Ambient in this case was approximately 70 °F and 35%-40% RH.

TABLE 8. FORMULATION FP_PU_3F

Item #	Material	Wet Wt. pound	Wet Vol. gallon	Wt. Solids pound	Vol. Solids gallon
1	Lumiflon L200 (60% resin solids)	38.4	4.08	23.0	1.96
2	Desmophen 670A-80	28.8	3.13	23.0	2.35
3	TiO2, Pure R 960 (white)	27.5	0.85	27.5	0.85
4	Bayferrox 3420 (yellow)	0.52	0.02	0.52	0.02
5	Light Blue 100 (blue)	0.67	0.02	0.67	0.02
6	Tint Ayd ST8317 (28% carbon black)	2.71	0.28	0.76	0.04
7	Byk 110	5.53	0.65	2.66	0.28
8	Tinuvin 292	0.71	0.07	0.71	0.07
9	Tinuvin 1130	0.71	0.09	0.71	0.09
10	1% T12 in 2,4 pentanedione	0.42	0.05	0.00	0.00
11	Desmorapid PP	0.04	0.01	0.04	0.01
12	Methyl n-amyl ketone (MAK)	27.7	4.07	0.00	0.00
13	Acetone (not counted in VOC)	49.0	7.43	0.00	0.00
14	Syloid 620	13.7	0.82	13.7	0.82
15	Fluo HT-LS	1.31	0.07	1.31	0.07
16	Isocyanate of HDI	27.3	2.90	24.6	2.53
	Total	225	24.5	119	9.11

weight solids (%)=53.0   P/B=0.63
volume solids (%)=37.1   PVC (%)=21.0
NCO:OH =1.60   VOC (g/l)=397 (3.34 lb/gal)
(Component I/Component II)=7.24

Laboratory film tests that are believed to possess predictive power with regard to film durability include certain measures of film hardness and resistance to scratching and marring. Cleanability is gauged through measurement of changes in color and gloss sustained in a prescribed dirtying-cleaning cycle performed on flat test panels. Properties degradation by fluids or gases is gauged through hardness and color measurements performed before and after exposure of the coating sample to the fluid for a prescribed time at temperature. Another type of test deemed relevant to performance in the field but which is not included in this study is measurement of the coating erosion rate sustained in a high kinetic energy water stream.

It is noteworthy that many topcoat properties probed in laboratory measurements will depend to varying degrees on the primer and underlying composite or metal oxide structure inclusive of any conversion coating or surface treatment given the metal, and on application parameters like cure time, application technique, and environment. The Battelle tests endeavor to probe certain of these variables. The data presented herein correspond to a single primer and single conversion coated aluminum alloy and temper.

The Battelle tests[24] appraised film hardness and wear through the Hoffman Scratch Test. The results for the three test coatings are shown in Figure 37. The growth of film hardness with time evident in Figure 37 reflects the degree of cure achieved following creation of the film through spraying. The TJF Solutions fluoro polyester urethane alloy exceeds by wide margins the polyester urethane and fluoropolymer urethane in the Hoffman measure of hardness/wear at all stages of cure.
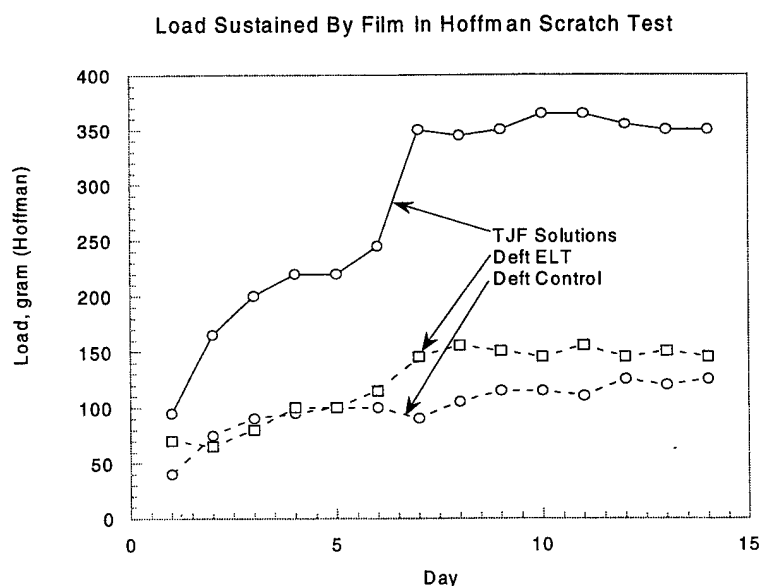
Figure 37. Battelle Hoffman Scratch Test results for three topcoat systems.

The Battelle tests[24] appraised relative fluid resistance to liquid water and humidity through before and after measurements of MAR and Hoffman Scratch. Both tests are

believed to gauge hardness and wear. Cleanability was gauged through a scrub test utilizing three different kinds of cleaning fluids differing in chemical activity and in traditional usage. The results for fluid resistance and cleanability for the three test systems are summarized in Tables 9 and 10, respectively.

Table 9. Battelle appraisal of water and humidity resistance through Hoffman and MAR tests.

	Deft Control		Deft ELT		TJF Solutions	
	Before	After	Before	After	Before	After
Water Immersion[1]						
2 day cure on film:						
Hoffman, gram	75	105	65	95	165	315
MAR, gram	30	45	25	50	65	250
14 day cure on film:						
Hoffman, gram	130	145	145	165	350	380
MAR, gram	55	95	70	85	400	560
Humidity Immersion[2]						
2 day cure on film:						
Hoffman, gram	75	100	65	90	165	345
MAR, gram	30	100	25	85	65	410
14 day cure on film:						
Hoffman, gram	130	150	145	150	350	405
MAR, gram	50	75	70	100	400	400

1. Water immersion is 96 hours, 120 ^{0}F.
2. Humidity 168 hours, 98% RH, 100 ^{0}F.

Table 10. Battelle appraisal of cleanability through scrub test with three different cleaning fluids.

Cleaning Fluid	Deft Control	Deft ELT	TJF Solutions
ALK 660[1]	47	17	75
B&B Regal[2]	81	25	90
Armakleen M-Aero-NS[3]	86	52	97

1. MIL-C-87937 Type II cleaner, 'Light Duty'. ALK 660 is typed a poor cleaner by Maintainers.
2. MIL-C-87937 Type III cleaner, 'Thixotropic Gels', not for general aircraft cleaning rather is meant for wheel wells, and like items.
3. MIL-C-87937 Type IV cleaner, 'Heavy Duty', recommended by Corrosion Office.

The Hoffman Scratch and MAR data of Table 9 offer insight into the development of fluid resistance with cure as well as a comparative measure of the steady state (i.e. full cure) resistance of the three test systems to deleterious effects of liquid water and 98% humidity. Generally, the two measurements are seen to reflect the same trends and

support similar conclusions. The two fluoropolymer containing urethane systems show a greater sensitivity to both liquid and gaseous water at low cure than does the polyester urethane system. Water tends to accelerate cure. The sensitivity of the test results to liquid and gaseous water is much reduced at the full 14 day cure for all three coating systems. However, the two Deft systems compare quantitatively and show less than half the Scratch and MAR resistance of the TJF Solutions fluoro polyester urethane alloy at 2 and 14 day stages of cure. Further comment would involve undue speculation.

The cleaning data of Table 10 show that the TJF Solutions alloy returns the highest marks of the three coating systems for all three cleaning fluids of the test matrix.

The final test of present interest in the Battelle series[24] reflects development of chemical resistance through the number of MEK (methyl ethyl ketone) wipes that the coating can sustain without damage. The test is run to a maximum of 100 wipes. The results for the three coating systems are given in Figure 38. Similarly to the Hoffman Scratch test results in Figure 37, these data indicate that the TJF Solutions polymer alloy cures faster than the polyester or fluoropolymer urethanes.

Number of MEK Wipes Sustained By Film
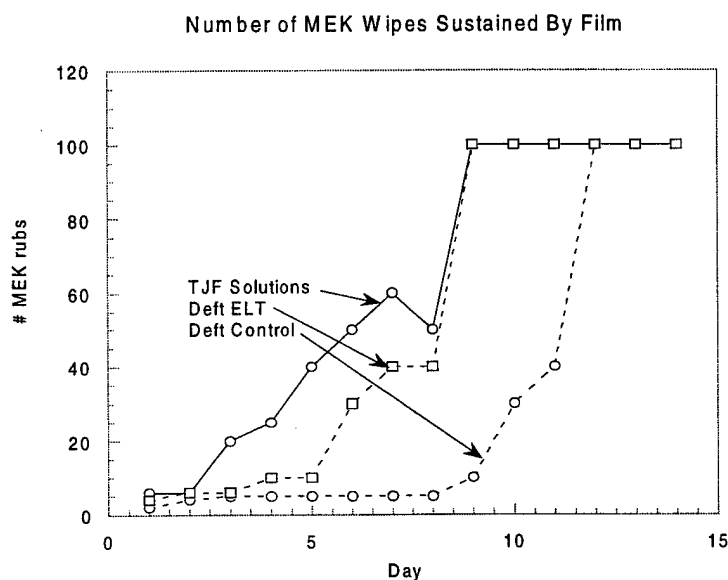
Figure 38. Battelle MEK wipes results for three topcoat systems.

Presumably, the superior performance of the TJF Solutions polymer alloy in the cited tests is attributable to a film structure featuring a stress bearing interface joining two distinct phases. The low surface energy fluoro urethane comprises the continuous phase and the higher surface energy polyester urethane comprises the included phase. It is further presumed that the distributions of the included phase particles in shape and size are important parameters. A validated theoretical description of the mechanism for distributing applied stress and impact energy among internal degrees of freedom that might explain the superior macro properties exhibited by the alloy is, however, lacking.

Nevertheless, certain polymer alloy properties become explicable with the realization that a single phase can dominate a test result when the property under test is sensitive to the presentation of that phase (i.e. as discreet or continuous at a surface). For example, the continuous phase dominates fluid resistance, and the continuous phase in the TJF Solutions polymer alloy system is a fluoropolymer urethane possessing intrinsically low solubility and diffusion coefficients. A property may at the same time depend sensitively on the volume concentration of a particular alloy phase. An example here is the rapid 'cure rate' of the TJF Solutions polymer alloy system compared to the Deft polyester urethane and Deft fluoropolymer urethane systems as manifested in the development of hardness and chemical resistance (Figures 37 and 38). If hardness and chemical resistance are viewed as extensive parameters that depend on the volume concentration of one or the other polyol, the faster cure rate appears as a consequence of the polymer alloy having half the unit volume of polyester or fluoropolymer urethane as the monolithic Deft systems. A satisfactory explanation for the disproportionate enhancement in film hardness and related properties like scratch resistance awaits the development of a comprehensive structural model for the polymer alloy.

In summary, the properties measurements suggest that the fluoro polyester urethane alloy can gain performance attributes beyond those of the parent fluoro and polyester urethanes in three ways. Extensive parameters can be controlled through adjustment in the unit volume of a critical phase. Intensive parameters can be engineered through selection of the constituent polyol chemical structures and film morphology. Finally, the phase interface can be engineered through choices in cross linking parameters.

5. Summary

A new approach to high performance ultra low gloss aircraft coating systems is described based on compatibilized immiscible blends of two polyols differing significantly in surface energy. Extensive characterization measurements show that the performance of the polymer alloy systems surpasses existing benchmark polyurethane and fluoropolymer topcoat systems in hardness, chemical, fluid, and abrasion resistance and cleanability. The superior performance is attributed to a favorable synergism between the parent homopolymers enabled by the stress bearing interface and morphology peculiar to a polymer alloy.

Microscopy performed on clear films shows that the 1:1 polymer alloy composition used in the pigmented topcoat system consists of spheroidal polyester urethane inclusions tens of micrometers in size within a continuous fluoro urethane matrix. The two polyols differ substantially, perhaps by as much as 0.2, in refractive index, and the inclusions lie in a size range that scatters visible and IR wavelengths. Surface and internal scattering by the included polymer phase lowers gloss substantially so that less extender pigment is needed than in conventional single phase polymer matrix systems to achieve ultra low gloss. Resin richness benefits many important coating properties. Light scattering measurements reveal a method for prescribing a size distribution of the included phase particles that will minimize specular reflection.

The large difference in polyol surface energies drives phase separation. The morphology realized in the dry film is strongly influenced by composition. The low surface energy fluoro urethane forms the continuous phase at fluoro:polyester polyol ratios below 1:3. The chemical bond strength of the fluoropolymer phase imparts superior chemical and UV radiation resistance to the coating and its lowered surface energy aids cleanability and mar and scratch resistance. The included polyester urethane phase lowers the time required to achieve maximum macro properties by reducing the mass of fluoro urethane present relative to a monolithic fluoropolymer matrix, e.g. by half in the 1:1 alloy. Some of the superior marks scored by the 1:1 two phase polymer alloy topcoat system in competitive performance tests follow directly from resin richness. Other property enhancements, for example film hardness and related properties like scratch resistance, benefited disproportionately in the alloy system for reasons that are as yet unclear.

Thermomechanical property measurements through DMA performed on thin films show directly the enhancement in film modulus enabled by the stress bearing interface connecting the separate phases that is a hallmark of polymer alloys. Pigmentation increases the storage and loss terms of the (complex) modulus and the glass transition temperatures of the alloys showing reinforcement with embrittlement.

It follows that means exist to correlate key coating properties from standard screening tests with more basic linear response coefficients derived from DMA to provide a more powerful model for coatings design. An example would be a quantitative expression of the change in film elasticity with pigmentation as gauged by GE Impact in terms of the

more fundamental (complex) modulus and glasslike to rubberlike structural transition. A correlation of structure to property of this caliber requires a more comprehensive rheology model than was accomplished in the present work.

Suggestions for extending and developing the polymer alloy concept for coatings are summarized in a list of recommendations.

*Thomas J. Fabish, TJF Technical Solutions, Inc., 4917 Simmons Circle, Export, PA 15632.
William F. Lynn, Veridian Engineering, 5200 Springfield Pike, Suite 200, Dayton, Ohio 45431.
Captain R. J. Passinault, 24th Training Squadron, Maxwell Air Force Base, Maxwell, Alabama 36112-6417.
Andrew Vreugdenhil, UDRI, 300 College Park, Dayton, Ohio 45469-0168.
Barbara Metz, Battelle, 505 King Ave., Columbus, OH 43201-2693.
Vince McGinniss, Battelle, 505 King Ave., Columbus, OH 43201-2693.

6. Acknowledgements

7. References

1. L.A Ultracki, "Thermodynamics And Kinetics of Phase Separation", Adv. Chem. Ser. (1994), 239 (Interpenetrating Polymer Networks), 77-123.

2. T.J. Fabish, "Fluorohydrocarbon-Urethane Alloys For High Performance Topcoat Systems; Initial Representation of Concept", a proposal to Materials Directorate, WPAFB, dated January 20, 1998.

3. Final Report, "LO Advanced Performance Coating Development and Demonstration, March 1 to January 31, 1998" [F33615-94-C-5803], T.J. Fabish, and November 1997, December 1997, and January 1998 Monthly Reports to Anteon Corp.

4. T.J. Fabish, "Fluorohydrocarbon-Urethane Alloys For High Performance Topcoat Systems; A Proof Of Concept Study", Final Report to Anteon Corporation for Period 15 April through 15 July, 1998, Report dated July 10, 1998.

5. J.L. Bantignies, G.Fuchs, G.L. Carr, P. Dumas, C. Wilhelm, Proc. SPIE-Int. Soc. Opt. Eng. (1997), 3153(Accelerator-Based Infrared Sources and Applications), 125-132.

6. A.M. Kaminski, M.W.Urban, *J.Coatings Tech.* **69** n872, 55-66 (1997).

7. M.W. Urban, C.L. Allison, C.C. Finch, B.A. Tatro, *J. Coatings Tech.* **71** n888, 75-85 (1999).

8. C.Wilhelm, J.L. Gardette, *J. Appl. Poly. Sci.* **51**, 1411-1420 (1994).

9. C. Wilhelm, J.L. Garette, *Polymer* **38** n16, 4019-4031 (1997).

10. G. Ellis, M. Claybourn, S.E. Richards, *Spec. Chim. Acta* **46A** n2, 227-241 (1990).

11. J.W. Hong, J.B. Lando, J.L. Koenig, S.H. Chough, S. Krimm, *Vibrational Spectroscopy* **3**, 55-66 (1992).

12. K.Palm, *Spec. Chim. Acta* **51A**, 1635-1642 (1995).

13. D. Lin-Vien, N.B. Colthup, W.G. Fateley, J.G. Grasselli, *The Handbook of Infrared and Raman Characteristic Frequencies of Organic Molecules*, , Academic Press, New York, 1991.

14. L.J. Bellamy, *The Infra-red Spectra of Complex Molecules (3e)*, Chapman and Hall, London, 1975.

15. C. D. Craver (ed), *Plasticizers and Other Additives (2e)*, Coblentz Society, 1985.

16. *An Infrared Spectroscopy Atlas for the Coatings Industry*, Federation of Societies for Coatings Technology, Philadelphia, 1980.

17. Stover, J. C., *Optical Scattering: Measurement and Analysis*, McGraw-Hill, New York, 1990.

18. van de Hulst, H. C., *Light Scattering by Small Particles*, Wiley, New York, 1957.

19. Kerker, M., Editor, *Selected Papers on Light Scattering, Part One*, SPIE Milestone Series, Vol. 951, Part One, 1988.

20. Kerker, M., Editor, *Selected Papers on Light Scattering, Part Two*, SPIE Milestone Series, Vol. 951, Part Two, 1988.

21. Flatau, P. J., http://atol.ucsd.edu/~pflatau/scatlib/, *Light Scattering Codes Library*, There are many useful links and references at this web site.

22. ScatCAD 4.0, Surface Optics Corp. ScatCAD is a derivative of CREEP, a software tool developed by USAF for modeling the scattering properties of lightly loaded coatings (thin films). ScatCAD incorporates multiple scattering effects using Kubelka-Munk theory.

23. Maxwell, J. R., J. Beard, S. Weiner, D. Ladd, and S. Ladd, "Bidirectional Reflectance Model Validation and Utilization," Technical Report AFAL-TR-73-303, Wright-Patterson AFB, 1973.

24. Battelle comparative testing of Deft Control, Deft ELT, and TJF Technical Solutions alloy is documented in internal Battelle reports. For further detail contact B. Metz, Battelle, Columbus.

8. List of Recommendations

1. The most influential factor affecting film performance properties in polymer alloy systems is the dry film morphology. It is important to elucidate the dependencies of film morphology on polyol structure, composition, and formulation methodology. A reasonably transparent correlation of morphology with independently measurable quantities like polyol surface energy, molecular weight and dispersion, and with incorporation parameters like shear energy would provide a basis for constructing an empirical design model for polymer alloy systems having limited but nevertheless useful predictive power.

2. Develop the correlation of scattering with the size distribution of included phase particles that is suggested in the present study by making and measuring films of appropriate composition. A validated model would enable specification of a distribution of inclusion sizes that optimize internal scattering for many systems of interest, alloy or monolithic polymer. In so doing, it is important to learn how to treat surface roughness in light scattering so that internal and surface structures may be designed together to meet minimum specular reflection standards.

3. Exploit the method suggested in the present study for connecting standard coating screening test results to more fundamental property measurements that can introduce the film structure into the correlation. For example, the GE Impact measure of elongation and MAR and Hoffman measures of wear and scratch resistance may be related to thermomechanical response coefficients measured in thin film DMA, microindentor hardness, surface energy, and coefficient of surface friction. This task requires an expanded scope for alloy rheology characterization measurements and adding other surface science characterization measurements to the litany of paint film screening tests. Success in correlating structure with properties would support construction of a design model for coatings that possesses broad predictive power. Validated models would significantly aid exploitation of new concepts in conductive coatings, primers, long lived topcoats, and specialized coatings for signature control.

4. Learn if the thermodynamic drive arising from the difference in polyol surface energies is sufficient to promote self-assembly of pigment particles. Success would provide a means to engineer the effective medium optical and transport properties (thermal and electrical) at minimal pigment loading which would coincidentally enhance all other film properties stemming from resin richness.

5. The manner in which a multiphase structure distributes applied stress or strain and impact energy among its internal degrees of freedom needs to be elucidated through theoretical modeling. Continuum mechanics and fracture mechanics might provide a basis for understanding the superior macro properties exhibited by the polymer alloy systems in various tests that probe mechanical properties.

Appendix A. Vibrational Spectroscopy of the Fluoro and Polyester Polyols and their Urethanes

Lumiflon 200

Lumiflon 200 is a commercially formulated fluoropolymer. Little else was known about its components so a vibrational analysis was carried out. This included infrared and Raman investigation of dry, uncured and HDI cured samples. The resulting spectra are shown in Figure A1 and Figure A2. A tentative peak assignment is provided in Table A1. The Lumiflon 200 IR and Raman spectra both contain considerable amounts of CH stretching intensity (2800-3000 cm^{-1}) suggesting that the polymer backbone is made up of at least equal amounts of fluorocarbon and hydrocarbon. The presence of an almost resolved shoulder at 2978 cm^{-1} (IR) and 2965 cm^{-1} (Raman) indicates that the sidechains include methyl terminations. The absence of a strong $(CH_2)_n$ rock at 720 cm^{-1} in the uncured polymer indicates that there are no long linear hydrocarbon chains in the system. This suggests that the non-cyclic sidechains are not longer than n=4.

Lumiflon does contain a large amount of alcohol functionality before it is cross linked as indicated by a broad feature at 3396 cm^{-1} (O-H stretch, IR) and the peaks at 1385 and 1090 cm^{-1} (C-OH bend, C-C-O stretching, IR). The uncured polymer also exhibits the expected CH_2 deformations between 1482 and 1346 cm^{-1} (IR and Raman) as well as a multi-peak envelope between 1260 and 1190 cm^{-1} that corresponds to C-C and C-F coupled vibrations. The Raman spectra shows typically strong well resolved peaks for the C-F,C-C vibrations at 1305, 1263, 1025 and 798 cm^{-1}.

Upon curing with HDI, the infrared OH stretch at 3396 cm^{-1} decreases in intensity and three infrared bands due to N-H stretching (3458, 3328 and 3134 cm^{-1}) are observed. These are consistent with the mono-substituted amide linkages present in a poly-urethane. The region between 1800 and 1400 cm^{-1} contains the most obvious series of infrared peaks assigned to the urethane formation. The most intense peak at 1690 cm^{-1} is due to the amide I or v(C=O). This peak has a strong shoulder at 1719 and a weaker shoulder at 1637 cm^{-1}. These three peaks are due to the different types of carbonyl species present. The band at 1637 cm^{-1} is indicative of poly-urea. The other two carbonyl peaks are usually assigned to free and hydrogen bonded carbonyls. In the Lumiflon and Desmophen system the relative intensity clearly depends on the composition of the system. This is described in more detail in the discussion of the blended systems. In the case of the Lumiflon system, the lower energy, H-bonded carbonyl dominates. In the Raman spectrum only one carbonyl peak is present for the HDI cured Lumiflon. This is assigned to the C=O stretching of the HDI isocyanurate ring at 1758 cm^{-1} and is a valuable indicator in the analysis of the polymer alloys.

Two other infrared peaks in this region that arise from the cure process are the amide II or C-N, C-N-H combination at 1518 cm^{-1} and the CH_2 deformation of the hexamethylene chains of the HDI at 1462 cm^{-1}. The band that appears at 760 cm^{-1} also arises from the cross linking reaction. This is due primarily to the N-H wag of the urethane linkages.

The infrared C-F stretches and CH_2 deformations are still found at 1260-1190 and 1482-1342 cm^{-1} respectively. The C-C-O stretching region undergoes some changes due to the reactions of the alcohol functionality and the creation of ester linkages. This effect can be observed in the dramatic decrease of the alcohol C-C-O IR stretch at 1090 cm^{-1}. The peak due to the ether linkage remains at 1070 cm^{-1} indicating that it arises from the unreacted sidechains. The disappearance of two Raman bands at 1121 and 1054 cm^{-1} also occurs upon curing which suggests that these bands are related to the C-O stretching of alcohol species in the uncured polymer.

Lumiflon 552

Lumiflon 552 is similar in many respects to Lumiflon 200 and as a result it shares many of the vibrational characteristics described above. Lumiflon 552 is a weaker Raman scatterer than the other materials in this study. This makes the identification of the weaker bands in the Raman spectra less reliable and its detection in polymer alloys more difficult.

A tentative list of infrared and Raman assignments is presented in Table A2. One striking feature of the IR and Raman spectra is the ratio of the intensities of the CH_2 asymmetric band at 2936 cm^{-1} to the asymmetric CH_3 band at 2969 cm^{-1}. The well-resolved CH_3 peaks suggest that there are a large number of methyl terminated side chains in the 552 resin. Upon curing, the additional CH_2 intensity due to the HDI methylene chains reduce this peak to a shoulder.

The IR spectra of Lumiflon 552 contain an intense band envelope between 1170 and 1000 cm^{-1} that is comparable to that observed at 1270-1150 cm^{-1} for the Lumiflon 200. By analogy these peaks are assigned to the C-F/C-C related bands. The region in the 552 is overlapped with a number of C-C-O and C-OH bands that change with curing. This is responsible for the observed differences in the spectra before and after curing. This shift in the fluorocarbon bands suggests that there are some differences between the compositions of the Lumiflon 552 and 200 systems. This is consistent with the known differences of the physical properties of the two resins.

Desmophen 670A-80

The infrared and Raman spectra for uncured, dried and HDI cured Desmophen 670 samples are shown in Figures A3 and A4. The related peak assignments are presented in Table A3.

The bands in the regions 3000-2800, 1258-1074 and 1050-850 cm-1 indicate the C-H, C-O and C-C functionality of the resin respectively. The weak C-H aromatic stretch at 3077 and the two overlapping aromatic ring stretches at 1608 and 1590 cm-1 indicate the aromatic content of the polyester.

As the base resin itself contains ester linkages, the carbonyl region of the spectrum ($1770-1630$ cm^{-1}) is more complex than that of the Lumiflon system. The uncured Desmophen exhibits two infrared and one Raman C=O bands. The infrared bands at 1735 and 1706 cm^{-1} can be assigned to ester and carboxylic acid carbonyl stretching motions respectively. The Raman spectrum contains only a single carbonyl band at 1722 cm^{-1} that is assigned to the carbonyl component of the polyester linkages as it is not affected by the curing process.

After curing with HDI, the Raman spectrum contains a second carbonyl band at 1757 cm^{-1} that is assigned to the carbonyl stretching of the five membered isocyanurate component of the HDI. As expected, the CH$_2$ deformations at 1477 and 1440 cm^{-1} increase with the addition of the HDI alkyl groups.

The changes upon curing are more pronounced in the infrared spectra. As observed in the Lumiflon system, the carbonyl region contains a number of overlapping bands. The two most prominent absorbances are assigned to the free (1720 cm^{-1}) and hydrogen bonded (1681 cm^{-1}) carbonyl stretches. In this case the most intense band is due to the free carbonyl species. Another important indicator of the cure in the infrared is the presence of the broad band at 1527 cm^{-1} which is assigned to the combination of the N-H deformation and the C-N stretch, commonly referred to as the amide I band. The O-H bending band at 1307 cm^{-1} also undergoes a substantial decrease in intensity as the alcohol functionality is consumed in the formation of polyurethane bonds.
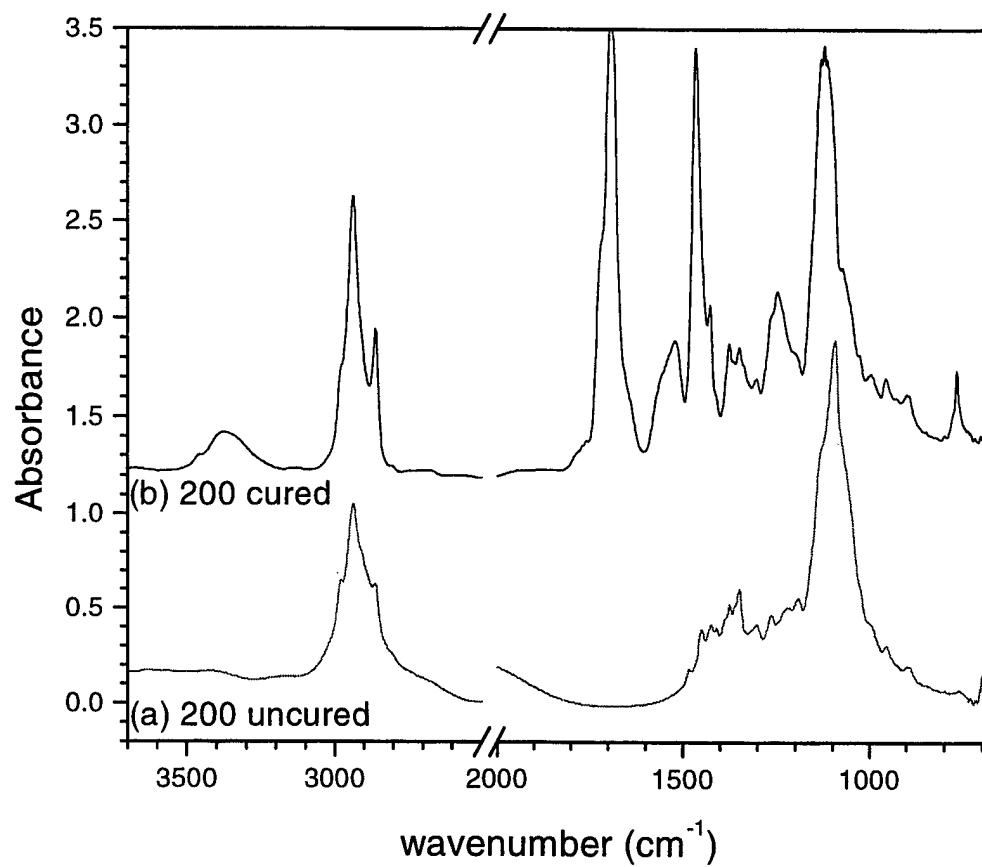
Figure A1. IR spectra of Lumiflon 200 (a) uncured and (b) cured.
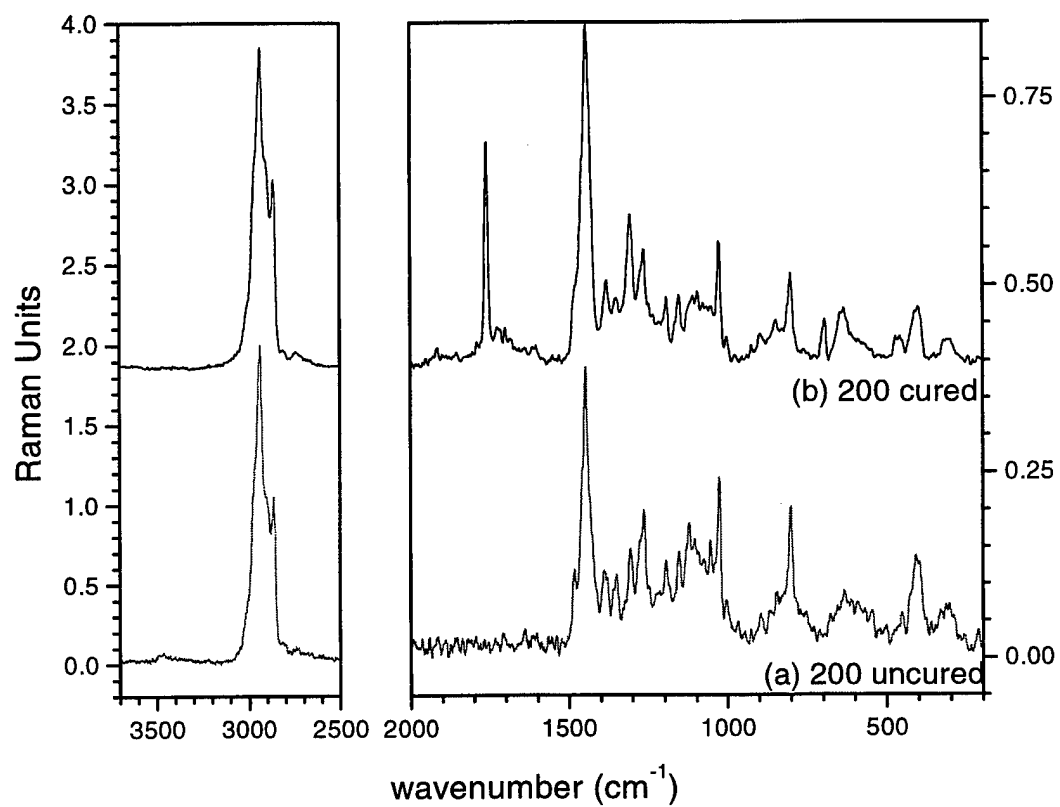
Figure A2. Raman spectra of Lumiflon 200 (a) uncured and (b) cured.
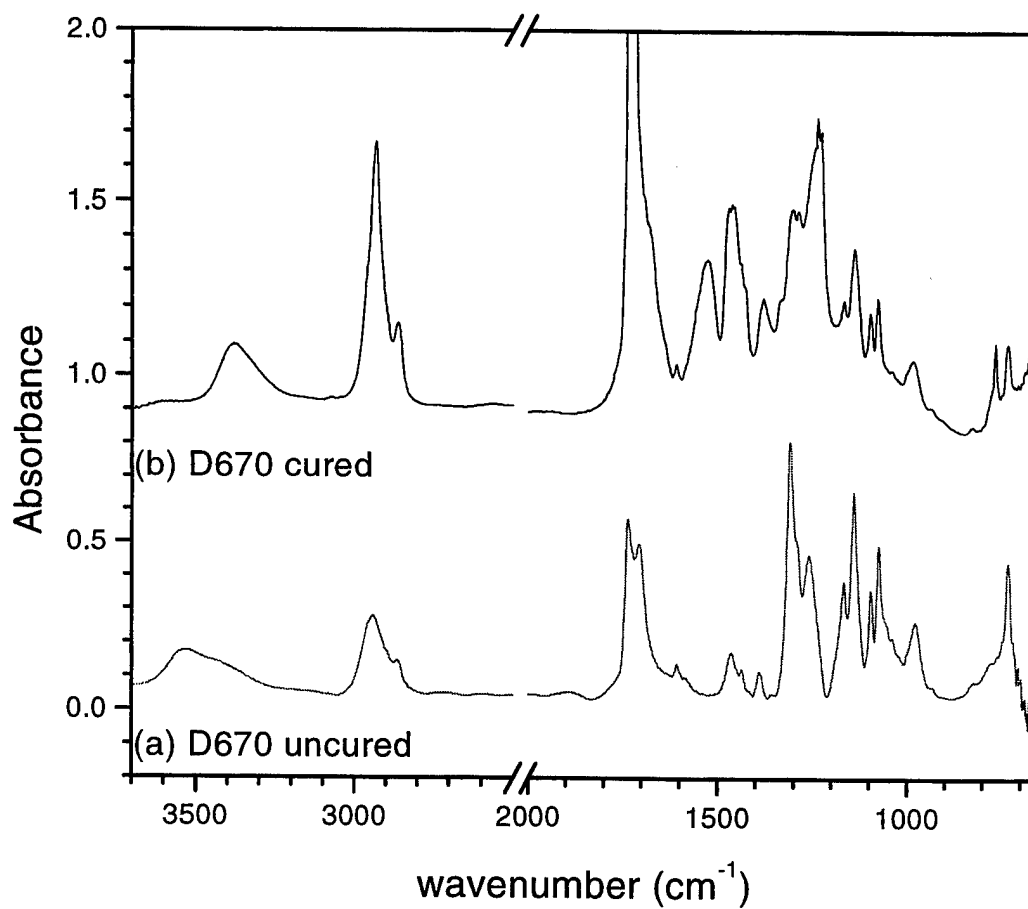
Figure A3. IR spectra of Desmophen 670A-80 (a) uncured and (b) cured.

Figure A4. Raman spectra of Desmophen 670A-80 (a) uncured and (b) cured.

Table A1: Proposed Assignments for Lumiflon 200.

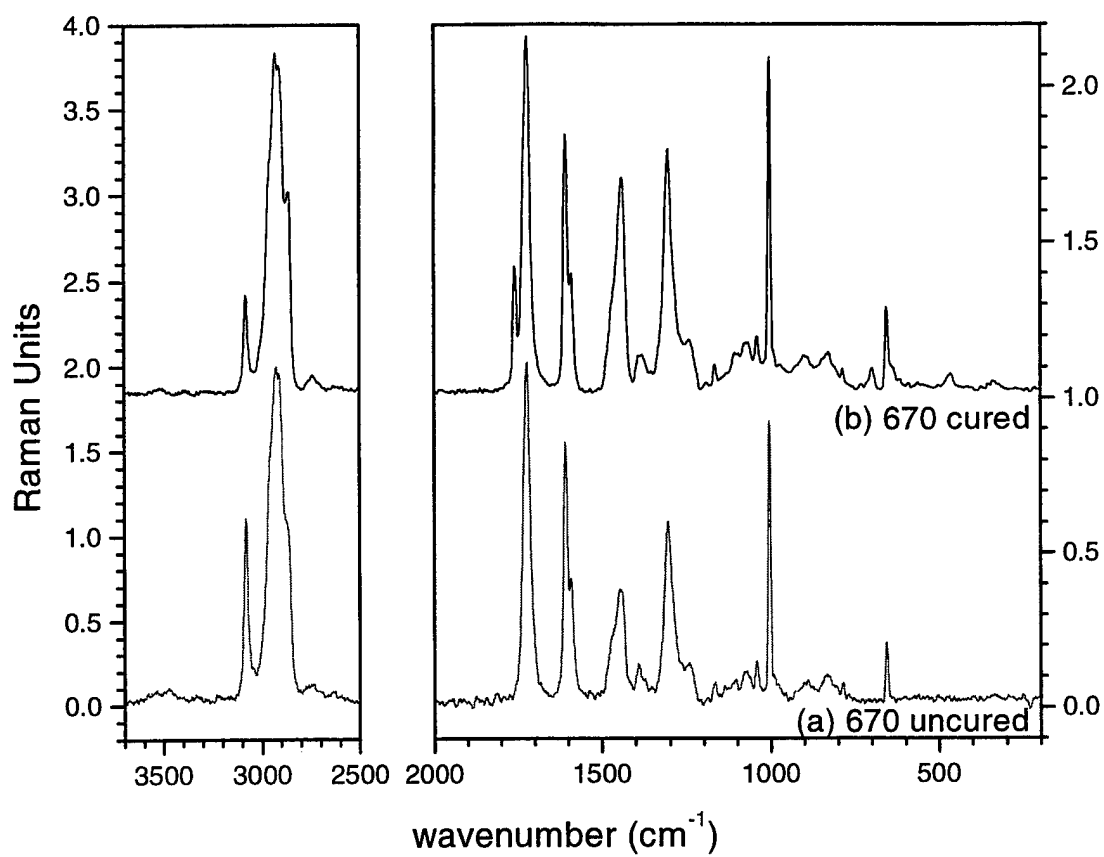| Mode	Uncured L200 IR	L200 IR	Uncured L200 R	L200 Raman	HDI IR
ν N-H		3458			
H-bonded ν O-H	3396	3371			
H-bonded ν N-H		3328			
$ν_a$ CH$_3$	2978	2978		2965	
$ν_a$ CH$_2$	2931	2935	2935	2935	
$ν_s$ CH$_3$	2908			2902	2939
$ν_s$ CH$_2$	2862	2859	2862	2859	2862
ν NCO out of phase					2269
ν C=O (free) HDI				1758	1760
ν C=O Free		1719			
ν C=O H-Bonded		1690			
δ N-H + $ν_s$ C-N amide II		1518			1511
δ CH$_2$	1482		1481	1479	
δ CH$_2$	1448	1462	1446	1444	1465
δ CH$_{2 +}$ ν NCO in phase	1423	1425			1430
δ CH$_2$	1409	1410			
C-OH Bend	1385		1389		
δ CH$_3$	1373	1374		1379	1374
δ N-H + $ν_s$ C-N					1357
ν C-F	1346	1346	1350	1350	
ν NC=O isocyanurate ring		1340			1340
γ CH$_2$	1299	1301	1306	1305	1304
CF2 Combo	1260	1261	1263	1263	
ν C-O ester		1243			1249
CF2 Combo	1196	1198	1194	1192	
C-O ether str	1130	1130	1154	1152	
$ν_a$ C-N-C HDI					1143
ν C-F		1118	1107	1108	
ν C-C-O out of phase alcohol	1090		1054		
ν C-C-O out of phase ester		1070			
ν C-C	1026	1025	1025	1025	
ν C-C	994	994	1002	1002	
ν C-C	954	951			
CF2	890	898		893	
$ν_s$ C-N-C HDI					861
ν C-C	862				
ν C-C	846			846	
ring vibration			799	798	
N-H wag		763			767
CH$_2$ rock		730			

Table A2: Proposed Assignments for Lumiflon 552.

| Mode	Uncured L552 IR	L552 IR	Uncured L552 Raman	L552 Raman	HDI IR
H-bonded ν O-H	3369	3369			
ν_a CH$_3$	2979	2974	2974	2969	
ν_a CH$_2$	2935	2934	2936	2936	2939
ν_s CH$_3$	2900		2894	2904	
ν_s CH$_2$	2860	2860			2862
ν NCO out of phase					2269
ν C=O (free) HDI				1758	1760
ν C=O Free		1721			
ν C=O H-Bonded		1690			
ν C=O Urea		1640			
δ N-H + ν_s C-N amide II		1521			1511
δ CH$_2$	1483			1483	
δ CH$_2$	1444	1465	1458	1443	1465
δ CH$_2$+νNCO in phase	1424	1426			1430
δ CH$_2$	1410	1410		1411	
C-OH bend	1389				
δ CH$_3$	1374	1375	1375	1379	1374
δ N-H + ν_s C-N					1357
ν C-F	1346	1349		1349	
ν NC=O isocyanurate ring		1338			1340
γ CH$_2$	1301	1300		1306	1304
CF2 Combo	1261	1262			
ν C-O ester		1244			1249
CF2 Combo	1193	1198			
ν_a C-N-C HDI					1143
ν C-F	1113	1121	1122		
ν C-C-O out of phase alcohol	1092				
ν C-C-O out of phase ester		1062			
ν C-C	1055	1055			
ν C-C	992	992			
ν C-C	951				
CF2	897	898			
ν_s C-N-C HDI					861
N-H wag		763			
CH$_2$ rock		735			

Table A3: Proposed Assignments for Desmophen 670A-80.

Mode	Uncured D670 IR	D670 IR	Uncured D670 Raman	D670 Raman	HDI IR
Free ν O-H	3528				
H-bonded ν O-H		3375			
ν CH aromatic		3073	3077	3077	
ν_a CH$_2$	2939		2929	2930	
ν_s CH$_3$			2909	2906	2939
ν_s CH$_2$	2863	2862	2862	2858	2862
ν NCO out of phase					2269
ν C=O Free (HDI)				1757	1760
ν C=O Free	1735	1720	1722	1721	
ν C=O carboxylic acid	1706				
ν C=O H-Bonded		1681			
ν C=O urea		1637			
ν C-C aromatic	1607	1607	1607	1607	
ν C-C aromatic	1584		1591	1590	
δ N-H + ν_s C-N amide II		1527			1511
δ CH$_2$	1463	1458		1477	1465
δ CH$_{2+}$ ν NCO in phase	1435	1436	1446	1439	1430
δ CH$_2$		1426			
δ CH$_2$	1386		1391	1381	
δ CH$_3$		1372			1374
δ N-H + ν_s C-N					1357
ν NC=O isocyanurate ring		1332			1340
δ OH	1307	1301			
γ CH$_2$		1286	1303	1303	1304
ν C-O ester	1258	1249	1241	1239	1249
ν C-O ether	1166	1166	1166	1165	
ν_a C-N-C HDI					1143
C-O ester related	1139	1137		1135	
ν C-C-O out of phase ether	1094	1095	1103	1102	
ν C-C-O out of phase alcohol	1074	1075	1072	1065	
ν C-C		1038	1041	1038	
ν C-C	978	982	1003	1002 strong	
longitudinal acoustical vibration			888	894	
ν_s C-N-C HDI					861
ν C-C			834	829	
N-H wag		766			767
CH$_2$ rock	733	730			

74

## Appendix B. Light Scatterometer Parameters and Error Analysis

Measurement of the four scattering parameters appearing in the governing equation for the experiment, $f = P_s / [P_i \Omega \cos(\Theta_s)]$, is the source of error and is influenced by multiple effects. A summary of these effects as they relate to the four measurement parameters is presented Tables B1 through B4. The errors associated with the measurement of incident power and scattered power are nearly identical, except that the former are not affected by receiver aperture misalignment and FOV nonuniformity. Errors are summarized in Table B5. The noise-equivalent BRDF (NEBRDF) for the hemispherical scatterometer at near-normal receiver angles are presented in Table B6. NEBRDF is inversely proportional to the cosine of the receiver angle. As a result, NEBRDF increases as the receiver angle approaches the grazing limit. The error analysis assumes that the material under investigation is homogeneous and isotropic.

The TMA laser scatterometer provides full-hemisphere coverage for angles of incidence reaching to extreme grazing angles (89 degree) at laser wavelengths corresponding to the five spectral regions that are important to materials development and signature evaluation. The five spectral regions are: UV (0.325 μm), visible (0.6328 μm), near IR (1.06 μm), and the two thermal IR atmospheric transmission windows, 3 - 5 μm and 8 - 14 μm (3.39 μm and 10.6 μm, respectively). All lasers are commercially available and were selected to optimize stability and lifetime and minimize maintenance. The level of automation incorporated allows the operator to write and link a series of up to 21 scan-definition files (SDF). Each SDF can collect BRDF data as a function of two nested variables. When the SDF are linked, data collection occurs without the intervention of an operator. Figure 13 illustrates the automated mechanical apparatus used to control the angles of incidence and reflectance--a goniometer. Two degrees of freedom are included in the sample holder for controlling the angle of incidence relative to the fixed incident-radiation axis. Two degrees of freedom also exist in the receiver for controlling the angle of reflectance.
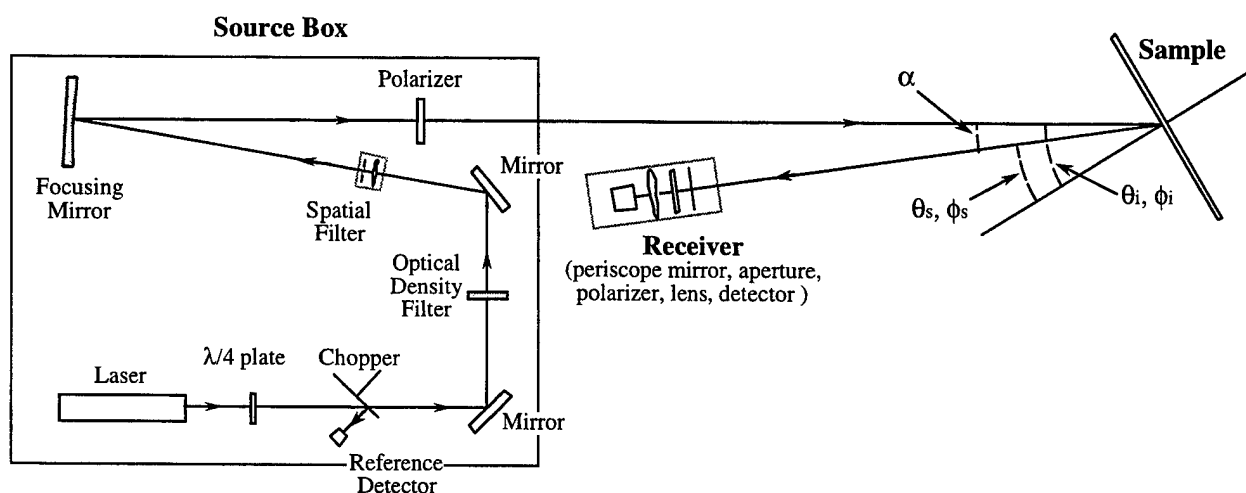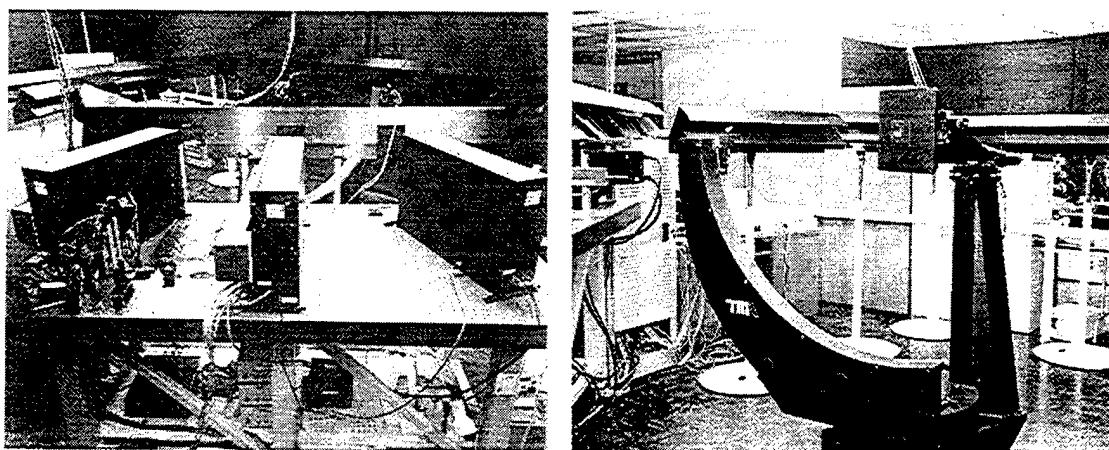
Figure B1. Illustration and schematic optical layout of the laser hemispherical scatterometer.

The receiver for the 1.06 μm laser used for this study is shown in Figure B1. A periscope mirror is the first element in the receiver and folds the optical path. The folded path eliminates obscuration of the incident laser radiation by the remainder of the receiver system and allows data collection to within ± 1.5 degree of the incident angle. However, the periscope mirror introduces a systematic polarization error in the measurements. This error is compensated by characterizing the reflectance properties of the mirror and correcting the data.
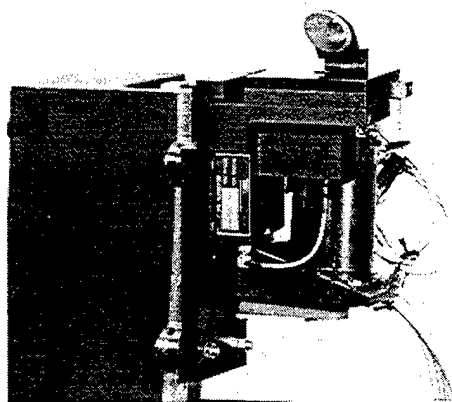
Figure B2. Receivers for the laser hemispherical scatterometer.

Table B1. Table of errors associated with the measurement of scattered power

Error Source	Error Type	Discussion
Receiver/Source Polarization	Systematic	Generally $\ll 0.1\%$. Only significant for samples which maintain or slightly rotate the polarization of the incident source. The error is greatest when measuring the cross-polarized component and is mainly a problem when measuring mirrors.
Receiver Aperture Misalignment	Systematic	Appears when measuring very near the specular direction and is mainly a problem when measuring mirrors.
Electronic and Detector Noise	Random	$\sim 1\%$ (1 std. dev.) and can be increased through integration time, except when approaching the NEBRDF of the instrument (which is easily observed in the data). The NEBRDF are measured at the maximum integration time and are $< 10^{-4}$ sr^{-1} (see Table 10).
Detector and Amplifier Nonlinearity	Systematic	$\sim 0.25\%$ (3 - 6 std. dev. for UV-VIS-NIR, 2 std. dev. for IR wavelengths).
Periscope Mirror Polarization Compensation	Systematic	$< 1\%$.
FOV Nonuniformity	Systematic	The effect of FOV nonuniformity at grazing angles was characterized during the preliminary and final design phases; near-incident effects were not studied. The FOV of each receiver is routinely measured. An engineering estimate of this error is $< 1\%$ (1 std. dev.) for the UV-VIS-NIR and 3.39-μm wavelengths when $\Theta_i < 80°$ and 10.6 μm when $\Theta_i < 60°$. For angles of incidence greater than these limits, the error is $\sim 2\%$ (1 std. dev.).
Aperture Nonuniformity	Systematic	This error was not characterized during the design phases. An engineering estimate of this error is $< 1\%$ (1 std. dev.). This error is calibrated with a combination of apertures for characterizing the nonuniformity. New calibration procedures based on integrated-BRDF and DHR measurements should reduce this error to $< 0.25\%$

Table B2. Table of errors associated with the measurement of incident power

Error Source	Error Type	Discussion
Aperture Effect	Systematic	This error occurs when the incident power is measured directly and the receiver aperture is smaller than the incident spot on the receiver. This error is extremely small for the TMA scatterometer.
Source Stability	Random	< 1% (2 std. dev.), except at 3.39 and 10.6 μm. The IR lasers are unstable and have power fluctuations which may be due to changes in their oscillation mode(s). These shifts appear to change the polarization or direction of the beam through the spatial filter and cause power variations at the sample which are uncompensated by the reference detector.

Table B3. Table of errors associated with the measurement of receiver solid angle

Error Source	Error Type	Discussion
Goniometer Alignment	Systematic	~ 0.5%. This error is the result of the uncertainty in the distance between the goniometer origin and the receiver aperture.
Sample Alignment	Random	~ 0.5%. This error is the result of the uncertainty in the placement of the sample at the goniometer origin.

Table B4. Table of errors associated with measurement of receiver elevation angle

Error Source	Error Type	Discussion
Goniometer Alignment	Systematic	This error is a function of Θ_s and increases as $\tan\Theta_s * \Delta\Theta_s$. The uncertainty in Θ_s is ± 0.02 deg. For angles as large as 80 deg, the error is < ± 0.2% (2 std. dev.). At 89 deg, the error is < ± 2%.
Sample Alignment	Random	This error is a function of Θ_s and increases as $\tan\Theta_s * \Delta\Theta_s$. The uncertainty in Θ_S is sample dependent but does not exceed ± 0.1 deg. For bistatic measurements where $-70° < \Theta_s < 70°$, the error is < 0.5% (2 std. dev.). For specular scans, Θ_s may be as large as 80°, and the error is < 1% (2 std. dev.). The error associated with the extraction of n and k from the specular-scan data is >> 1%. For verification scans, Θ_s may be as large as 85°, and the resulting error is < 2% (2 std. dev.).

Table B5. Summary table of errors

Error Source	Random	Systematic
Scatter Power	1 % (1 std. dev.)	2 % (> 2 std. dev.) 1 % (1 std. dev.) 1 % (1 std. dev.)
Incident Power	1 % (1 std. dev.) 1 % (1 std. dev.)	2 % (> 2 std. dev.) 1 % (1 std. dev.)
Solid Angle	0.5 % (2 std. dev.)	0.5 % (2 std. dev.)
Receiver Angle	0.5 % (2 std. dev.)	0.2 % (2 std. dev.)
Total	1.75 % (1 std. dev.)[†]	5.35 % (1 std. dev.)[†]

[†]It is assumed that the error at 2 std. dev. is twice that at 1 std. dev.

Table B6. Table of NEBRDF values for the laser hemispherical scatterometer

Wavelength	NEBRDFLaser Scatterometer
0.325 μm	1.0 E-5
0.6328 μm	1.0 E-7
1.06 μm	1.0 E-7
3.39 μm	1.0 E-4
10.6 μm	5.0 E-6